ENGINEERING α-1 PROTEINASE INHIBITOR TO TARGET PR3

ENGINEERING α-1 PROTEINASE INHIBITOR TO TARGET NEUTROPHIL SERINE PROTEINASE PR3

By AHMED AL-ARNAWOOT, B.H.Sc.

A Thesis Submitted to the School of Graduate Studies in Partial Fulfillment of the Requirements for the Degree

Master of Science

McMaster University

McMaster University MASTER OF SCIENCE (2020)

Hamilton, Ontario (Medical Sciences)

TITLE: Engineering α-1 Proteinase Inhibitor to Target Neutrophil Serine Proteinase PR3

AUTHOR: Ahmed Al-Arnawoot, B.H.Sc. (McMaster University)

SUPERVISOR: Dr. William P. Sheffield

COMMITTEE MEMBERS: Dr. Jonathan Bramson, Dr. Colin Kretz

NUMBER OF PAGES: xvi, 145

Lay Abstract

When harmful substances enter our body such as bacteria or viruses, we have ways of protecting ourselves from them. One of those ways is through a cell called the neutrophil. This is an immune cell that can release “fighting tools” into our blood to combat the harm. Some of these tools are called proteins. One of those proteins is Proteinase 3. However, sometimes our neutrophils can be activated without the presence of viruses or bacteria by products made in our bodies called autoantibodies. When this happens, too many of the “fighting tool” Proteinase 3 is released leading to damage to the tubes or vessels that our blood flows through. This project aimed to find a new possible way to stop these extra fighting tools from doing harm to our body. We did this by creating a library of different proteins that can stop Proteinase 3 once it is released by the neutrophil.

Abstract

Activated neutrophils release a neutrophil serine proteinase (NSP) called Proteinase 3 (PR3). In granulomatosis with polyangiitis (GPA), an autoimmune vasculitis, enhanced PR3 release results in endothelial damage. Serine proteinase inhibitors (serpins) such as α-1 proteinase inhibitor (API) inhibit NSPs through the serpin's reactive center loop (RCL). However, API is known to bind PR3 with a low specificity, compared to its main inhibitory target Human Neutrophil Elastase (HNE). The current treatment for GPA is immunosuppression, which leaves patients immunocompromised. Thus, the overall aim of this study was to engineer an API variant with a higher specificity to PR3 than HNE, which could serve as a possible novel therapeutic strategy for GPA.

We created an API expression library, hypervariable at RCL residues A355-I356-P357-M358-S359, and expressed it in a T7 bacteriophage display system. This phage library was then biopanned for PR3 binding. Two conditions were used for each round of biopanning: experimental, with PR3, and the negative control, without PR3. The library was biopanned for a total of five consecutive rounds, with the product of one screen serving as the starting material for the next. A bacterial mass lysate screen was also employed to further probe the library with PR3.

The phage-display and bacterial lysate screens resulted in the selection of two novel variants API-DA (D357/A358) and API-N (N359). Serpin-proteinase gel complexing assays indicated that API-N formed complex with PR3 similar to API-WT (wild-type), while API-DA was mainly cleaved as a substrate. There was no significant difference between the second order rate constants of API-N and API-WT reactions with PR3. Rate constants for API-DA binding to PR3 or for API-HNE reactions were not completed due to novel coronavirus (COVID-19)

restrictions. However, this project successfully demonstrated the ability to screen a hypervariable API phage library with PR3, yielding two new novel API variants.

Acknowledgments

I would like to thank my research supervisor Dr. William Sheffield whose guidance, mentorship and support were imperative to my success as a Master's student. His door was always open to me and he never hesitated in taking any of my questions. His humor and light-heartedness made my time at the lab more enjoyable. I could not have imagined a better supervisor and mentor. I would also like to thank my supervisory committee members Dr. Jonathan Bramson and Dr. Colin Kretz for their support and advice.

Working in this lab has been an incredible pleasure and I would like to especially thank Varsha Bhakta who taught me everything I know about lab procedure and experimental techniques, without whom my progress during this time would have been much slower. I also want to thank Louis Eltringham-Smith, Antje Ask, Dr. Syed Qadri, Dr. David "Kojo" Donkor, Mostafa Hamada, Jake McNairn and Anjali Patel for being incredible lab mates. The time we spent together and the conversations we had, whether about soccer, Game of Thrones or the latest tech, made me cherish my time in the lab.

Finally, I would like to thank my parents, Salah and Najwa, who always stood by me, supported me in my career choices, and whose advice I could always count on. Even though to this day they do not fully understand what I do, I want to thank my sisters Basma and Amna, and my brother Mohammed for their unconditional support. I also want to thank my friends who never said no to a FIFA game.

I look forward to the next chapter in my life!

Table of Contents

List of Figures

List of Tables

List of Abbreviations and Symbols

AAV	ANCA-associated vasculitis
ACT	α-1-antichymotrypsin
AMP	ampicillin
ANCA	anti-neutrophil cytoplasmic autoantibodies
API	α-1 proteinase inhibitor
API-R	API Pittsburgh variant
AS	antisense
bp	base pair
BSA	bovine serum albumin
cfu	clone forming unit
COVID-19	novel coronavirus
cPR3	complementary peptides to PR3
DA	D357/A358
DNA	deoxyribonucleic acid
E.coli	Escherichia coli
EXP	experimental
FRET	fluorescence resonance energy transfer
FT	Flow-Through
fXIa	factor XIa
GPA	Granulomatosis with Polyangiitis
GST	glutathione-S-transferase
HNE	human neutrophil elastase
HRP	horse radish peroxidase
HRV3C	human rhinovirus type 14 3C
IgG	immunoglobulin G
IL8	interleukin-8
IPTG	isopropyl β-d-1-thiogalactopyranoside
IV	intravenously
k_2	second order rate constant
k_2^*	uncalibrated second order rate constant
kDa	kilodaltons
kg	kilogram

LB	Luria Broth
LEI	leukocyte elastase inhibitor
M	molar
mg	milligram
MHC	major histocompatibility complex
mL	milliliter
mM	millimolar
MOI	multiplicity of infection
MPO	myeloperoxidase
MPO-GPA	MPO-mediated GPA
mPR3	membrane PR3
N	N359
n	sample size
NEG	negative control
NGS	Next Generation Sequencing
Ni-NTA	nickel chelate affinity
NSP	neutrophil serine proteinase
OD	optical density
ORF	open reading frame
ORI	origin of replication
P_0	starting concentration of PR3
PAGE	polyacrylamide gel electrophoresis
PAI-1	plasminogen activator inhibitor-1
PBS	phosphate buffered saline
PBS-T	PBS with Tween-20 0.1% v/v
PCR	polymerase chain reaction
PD	plasma derived
pfu	plaque forming unit
PI3K-AKT	phosphoinositide 3-kinase-protein kinase B
PI8	proteinase inhibitor 8
PMSF	phenylmethylsulfonyl fluoride
PR3	proteinase 3
PR3-GPA	PR3-mediated GPA
PRTN3	genes encoding PR3
P_t	unreacted PR3
RCL	reactive center loop
rpm	rotations per minute

RT	room temperature
s	second
S	sense
s1C	strand 1 on β-sheet C
s4A	strand 4 of β-sheet A
s5A	strand 5 of β-sheet A
ScFv	single chain variable fragments
SD	standard deviation
SDS	sodium dodecyl sulfate
SERPINB1	leukocyte elastase inhibitor
Serpins	serine proteinase inhibitors
$t^{1/2}$	half-life
T7Select10	T7Select capsid 10-3 protein
TBST	Tris-buffered saline containing Tween 20
TNF-α	tissue necrosis factor-α
U	unit
v/v	volume/volume
WT	wild-type
α	alpha
β	beta
µg	microgram
µL	microliter
µM	micromolar

Declaration of Academic Achievement

All of the work presented in this thesis was done independently by me, with the exception of creating the API-P2P1 phage library, which was generated by Dr. Benjamin Scott. This work was presented in preliminary form at the 8th Annual Norman Bethune Symposium in Vancouver, Canada, April 3, 2019.

1 Introduction

In this thesis, the engineering of a novel recombinant proteinase inhibitor was explored, with the long-term goal of inhibiting a specific proteinase involved in a serious illness, Granulomatosis with polyangiitis (GPA).

1.1 Granulomatosis with Polyangiitis

GPA, formerly known as Wegner's Granulomatosis, is an autoimmune vasculitis.[1] It commonly affects small to medium sized vessels and manifests as systemic necrotizing vasculitis, necrotizing granulomatous inflammation and necrotizing glomerulonephritis.[1] Its clinical signs usually present in the upper and lower respiratory tracts and the kidneys.[1] GPA has an incidence of 2.1-15 per million population equally distributed between males and females.[2] It is most common in individuals between the ages of 65 and 70 years.[2]

1.2 Pathogenesis of GPA

The pathophysiology of GPA begins with anti-neutrophil cytoplasmic autoantibodies (ANCAs). These are autoantibodies that specifically target antigens ordinarily stored in the cytoplasmic granules of neutrophils and lysosomes of monocytes, but which may be presented elsewhere during disease onset.[3,4] GPA is also known as an ANCA-associated vasculitis (AAV), which are a group of autoimmune vasculitis diseases provoked by the release of ANCAs.[3,4] The two main autoantigens of ANCAs in GPA are Proteinase 3 (PR3) and Myeloperoxidase (MPO), both stored in azurophilic granules in neutrophils.[3,4] These are proteins that are released when ANCAs bind to neutrophils and activate them (detailed mechanism is discussed in later sections). These proteins then

cause endothelial damage leading to vasculitis.[3,4] This paper will focus on PR3-mediated GPA (PR3-GPA). However, it is useful to understand the distinction between it and MPO-mediated GPA (MPO-GPA). Briefly, PR3-GPA generally affects the microvasculature in the lungs, while MPO-GPA is mostly restricted to renal vasculitis.[3,4] Furthermore, PR3-GPA is more common in northern parts of the world, whereas MPO-GPA is found in southern Europe and Asia.[4]

1.2.1 Source of ANCAs

The exact mechanism by which ANCAs are produced in the body is still unclear. However, evidence has shown that it could be due to a complex interaction between different stimuli.[3] The first stimulus is infection. In PR3-GPA, respiratory pathogens have been of interest in the genesis of ANCAs. Essentially, these pathogens (specifically *Staphylococcus aureus*) could produce complementary peptides to PR3 (cPR3).[5] These are the antisense coded peptides of PR3. A study has found that the adaptive immune system is capable of producing antibodies against cPR3, which in turn causes the production of cognate antibodies against PR3.[5] Thus, autoantibodies against PR3 are produced leading to their release and binding. Another factor that contributes to PR3-GPA pathogenesis is the existence of genetic mutations that predispose individuals to ANCA production and vasculitis. PR3-GPA is associated with single nucleotide polymorphisms in HLA-DP1, a gene complex that encodes major histocompatibility complex (MHC), and genes encoding PR3 (PRTN3) and α1-proteinase inhibitor (API), a serine proteinase inhibitor (serpin).[6]

1.2.2 Proposed Mechanism of PR3-GPA

Although this mechanism is not fully elucidated yet, the proposed sequence of events leading to GPA starts when circulating neutrophils are primed for activation by ANCAs by inflammatory cytokines or C5a, which is a component of the complement system.[7] This priming allows neutrophils to express ANCA autoantigens, in this case PR3 on their cell surfaces.[8-11] This PR3 is denoted membrane PR3 (mPR3). Although most of the PR3 is stored in azurophilic granules and secretory vesicles in neutrophils, there is a subset that is found as mPR3.[8] It should be noted however, that since PR3 is not a transmembrane protein, it binds to other cell surface receptors, such as CD177, to remain expressed on the plasma membrane.[12] mPR3 expression within patients can also be bimodal, with high-mPR3 and low-mPR3 expressing neutrophils.[8,9] This PR3 expression allows for ANCA binding to mPR3 followed by neutrophil activation. The activated neutrophils then release further C5a recruiting more neutrophils that undergo similar activation.[13,14] However, ANCA binding to mPR3 is not the only interaction required for neutrophil activation and subsequent degranulation. Neutrophil surface Fc receptor binding with ANCAs and the crosslinking of F(ab′)2 fragments can also occur.[15,16] Furthermore, ANCAs could also lead to neutrophil activation through the phosphoinositide 3-kinase-protein kinase B (PI3K-AKT) pathway.[17,18] This activation ultimately results in the release of PR3 from secretory vesicles and granules.[19] It has been shown that endothelial cells are capable of internalizing PR3 once it has been released into the plasma.[20] This PR3 is then localized to the nucleus, and becomes associated with

chromatin, which triggers apoptosis. Such observations provided further insight into how PR3 could lead to vasculitis and endothelial damage once released from neutrophils.[20]

1.3 Current GPA Treatment Strategies

GPA lacks a specific treatment; therefore, cyclophosphamide and corticosteroid combination therapy has been utilized since the 1970s.[1] Cyclophosphamide is a common chemotherapy drug used to suppress a variety of cancers.[21] It is an alkylating agent, with an active metabolite called phosphoramide mustard.[22] This active agent reacts with guanine and cytidine, leading to inter-strand crosslinks in DNA and acting as an anti-mitotic agent.[23] By targeting immune cells, cyclophosphamide leads to immunosuppression.[21,22] Corticosteroids on the other hand, are a class of commonly used anti-inflammatory drugs.[24] These steroid molecules bind to intracellular glucocorticoid receptors, forming a complex.[24] This complex is then internalized into the cell's nucleus where it binds to glucocorticoid response elements as dimers.[24] This binding results in inhibition of transcription factors that control the synthesis and expression of pro-inflammatory mediators such as macrophages, inflammatory cytokines and various interleukins.[24] Corticosteroids also upregulate annexin A1, which can reduce prostaglandin and leukotriene synthesis. This upregulation also inhibits cycolooxegenase-2 activity, which reduces neutrophil migration to sites of inflammation.[24] Due to their intracellular mode of action, the effects of corticosteroids are persistent even if their plasma levels are undetectable.[24]

This combination of immunosuppressive and anti-inflammatory therapy became the standard of care after Fauci et al. published their paper in 1983.[25] These investigators

found that prolonged cyclophosphamide treatment was effective in ANCA-related vasculitis, whereby 91% of patients showed improvement in disease status and 75% achieved sustained disease remission.[25] This remission, due to prolonged chemotherapy treatment, came with substantial risk. 46% of patients developed serious infection, 57% became infertile, and 43% developed hemorrhagic cystitis.[25] It was later found that pulsed cyclophosphamide (15 mg/kg intravenously (IV) every 2–3 weeks) produced similar remission results as prolonged cyclophosphamide, but with a reduction in risk.[26] However, the long-term probability of relapse in disease is higher with the pulsed regimen.[27]

To help sustain remission of disease in patients, rituximab has also been suggested as a substitute for cyclophosphamide.[21] Rituximab is a monoclonal antibody that binds to the CD20 receptor on B cells, causing antibody binding-mediated cytotoxicity.[28] Using this drug with corticosteroids is logical because B cells produce ANCAs, thus theoretically, this combination can reduce ANCA production and inflammation.[28] However, this reduction in B cells is transient and variable between patients.[28]

All of the current treatment strategies are immunosuppressive and leave patients susceptible to infection, even though rituximab has shown reduction in risk. There is a need for a non-immunogenic disease management strategy. Thus, downstream rather than upstream targets in GPA could be inhibited. One of those main targets would be PR3. This could be done by exploiting the body's natural inhibitor of PR3, API, which is a member of the serpin family of proteins.[29]

1.4 Serine Proteinase Inhibitors

Serpins are a superfamily of proteins.[30] They are not only found in mammals, but other animals, plants, bacteria and viruses.[30] The majority of serpins inhibit serine proteinases. However, some serpins can assume other roles such as hormone transporters, molecular chaperones and tumor suppressors.[30] Over 1500 members have been discovered with 34 being serpins found in humans.[30] Most serpins have a conserved primary structure of approximately 380 residues that fold into a single domain composed of three β-sheets (A, B and C) and 8 or 9 α-helices packed mostly on one side of the major β-sheet, sheet A (Figure 1).[30,31] The variability between different serpins lies within the reactive center loop (RCL).[30,31] This is an exposed loop on the surface of serpins that is critical for function. It is approximately 20-25 residues long and is linked to strand 5 of β-sheet A on the N-terminal end (s5A) and strand 1 on β-sheet C (s1C) on the C-terminal end (Figure 1).[30,31] The RCL contains the recognition scissile bond for target proteinases.[31] This sequence is named P1-P1' with residues towards the N-terminal labelled P1, P2, P3 and so on, and residues towards the C-terminal are labelled P1', P2', P3' and so on.[32] Although many residues within the RCL can control the specificity of a serpin, the P1 residue is a major determinant.[31] Altering the P1 residue allows serpins to inhibit different proteinases. For example, proteinase inhibitor 8 (PI8) inhibits trypsin-like proteinases by utilizing R339 (the predicted P1) as the P1 residue, and chymotrypsin-like proteinases by utilizing S341 (the predicted P2') as the P1 residue.[33]

Unlike traditional and canonical inhibitors, serpins utilize unique and extensive conformational changes that allow them to act as "suicide" or "single use" inhibitors of

proteinases.[30,31] The first change that occurs is the spontaneous folding of serpins into a metastable conformation (Figure 1).[30,31,34] This is the active or native conformation of serpins. In this form, the RCL exists as an extended loop on the surface of the protein.[30,31,34] Even though the native conformation is stable, the RCL itself can be unstable as an exterior loop.[30,31] To increase their stability, some serpins such as human plasminogen activator inhibitor-1 (PAI-1) can spontaneously enter a latent (inactive) conformation where the RCL is inserted into the center of β-sheet A as a fourth strand (s4A) (Figure 1).[30,31] This change occurs with the concomitant extraction of s1C. Although the depletion of strands in β-sheet C is energetically unfavourable, the insertion of s4A results in an overall gain in stability.[30,31] This principle was validated by an increase of 17°C in the denaturation temperature of latent PAI-1 compared to its native state.[34] The third and most stable conformation occurs with the cleavage of the RCL towards the C-terminal, at the P1-P1' bond (Figure 1).[34] This allows for the insertion of s4A into β-sheet A without the extraction of s1C from β-sheet C, thereby resulting in a very energetically favoured state. This cleaved state closely resembles the structure of the serpin portion of serpin-proteinase inhibitory complexes .[34]

Figure 1: Different Conformations of Serpins.

API is shown in this figure. (A) is the active/native conformation. (B) is the cleaved and (C) is the latent. The active conformation has the most potential energy thus the most unstable. This is followed by the latent, and finally the cleaved conformation which is the most stable conformation. When the RCL inserts into β-sheet A, it is designated as strand 4 of β-sheet A (s4A). The red indicates β-sheet A.[34]

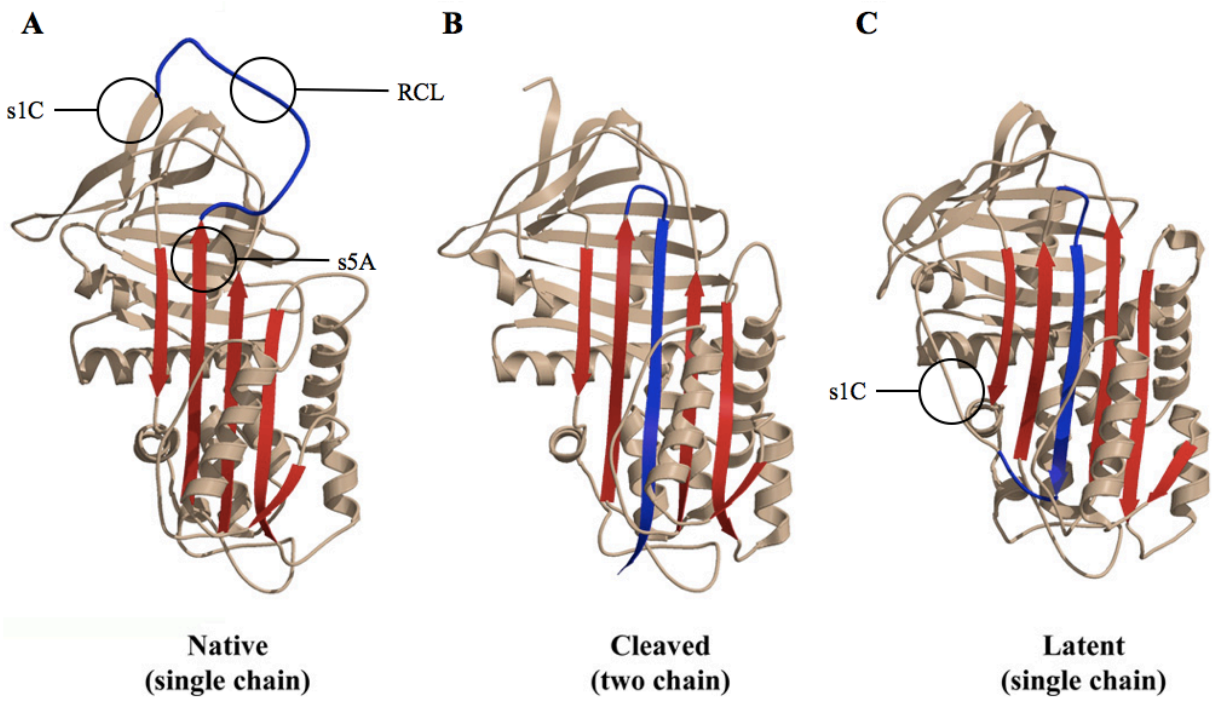
A
B
C
s1C
RCL
s5A
s1C
Native
(single chain)
Cleaved
(two chain)
Latent
(single chain)

1.5 Serpin-Proteinase Inhibition

When a proteinase binds to the RCL of a serpin, a non-covalent complex is formed that is similar to the "lock and key" complexes that form with classical inhibitors, and proteinase-substrate docking.[34] However, in the serpin-proteinase complex, after formation of a tetrahedral intermediate, the subsequent cleavage of the scissile peptide bond forms an acyl-enzyme intermediate.[35] With this cleavage, the energetically favourable insertion of the RCL into β-sheet A can occur.[34,36] As mentioned earlier, the proteinase binds to the C-terminal end of the RCL. Therefore, once the RCL is inserted, the proteinase will be pulled towards the distal or bottom end of the serpin along with the C-terminal end.[36] At this point, distortion and compression of the active site of the proteinase results in a kinetically trapped acyl-enzyme intermediate.[36] This, otherwise short-lived intermediate, is stabilized by a covalent linkage between the active site serine of the proteinase and the carbonyl of the cleaved RCL.[36] Furthermore, a fluorescence study has shown that the proteinase was partially unfolded in the final serpin-proteinase complex, further inhibiting its function.[37] The investigators demonstrated a rise in the fluorescence of the proteinase (in this case it was thrombin), which corresponded with the serpin-proteinase docking complex.[37] This initial increase was followed by a decrease in fluorescence of the proteinase, which corresponded with its translocation, due to the insertion of the RCL into the body of the serpin.[37] Since a serpin requires the cleavage of its RCL to inhibit proteinases, once present in a serpin-proteinase covalent complex, it can no longer be reused, explaining its description as a "suicide inhibitor".[34]

Moreover, for successful inhibition to occur, the serpin must enter its metastable state efficiently without transitioning into its latent state.[38] The RCL must be of an appropriate length to ensure the proper translocation of the proteinase without any slack to facilitate distortion of the proteinase's active site, which prevents serpin release from the complex.[39] Such a length is usually 17 residues on the N-terminal end of the P1-P1' cleavage site.[39] Furthermore, the translocation must occur rapidly enough to avoid deacylation. [40] Finally, the residues within the RCL need to be compatible with the folds in β-sheet A to ensure proper insertion.[41] If these conditions are not met, instead of forming a serpin-proteinase complex, the serpin will act as a substrate to the proteinase, resulting in an inactive cleaved serpin and an active proteinase, following attack by a water molecule and hydrolysis of the acyl intermediate.[34]

1.6 α-1 Proteinase Inhibitor

API, also called α-1 Antitrypsin, is the most abundant serpin present in human plasma, at 20-40 μM.[42] It is primarily synthesized in hepatocytes; however, monocytes and macrophages could also produce API.[43] Upon synthesis, a 24-amino acid pre-sequence peptide is produced, which is later eliminated through intracellular processing, leading to the production of a mature 394 amino acid polypeptide chain.[44] Furthermore, API has 3 N-linked glycosylation sites resulting in a 52 kDa glycoprotein.[43] It was the first serpin to have its structure solved using X-ray crystallography, which provided insight into RCL cleavage and insertion.[30] Its main inhibitory target is Human Neutrophil Elastase (HNE).[30] API became a major protein of interest due to the Pittsburgh mutation (API-R).[45] The mutation is so called due to its discovery in the fatal case of a boy from

Pittsburgh, Pennsylvania, who suffered from uncontrolled bleeding in the late 70s.[45] This mutation resulted in a single substitution of the P1 residue (M358) from methionine to arginine.[45,28] This change altered the specificity of API. The new API mutant became a potent inhibitor of procoagulant enzymes, including thrombin and factor XIa (fXIa), thereby leading to a hemorrhagic disease.[45,46] This case provided insight into the importance of the P1 residue in determining serpin specificity.[30,31]

API deficiency can also result in other diseases throughout the body. This can occur due to the Z-mutation, in which a lysine substitutes for a glutamic acid residue at position 342 at the top of β-sheet A.[34,47] Such a substitution causes an increase in instability in the protein, which leads API to polymerize. In this scenario, the RCL of one API inserts into β-sheet A of another API and so on till a chain of inactive APIs is formed.[34] Because API ordinarily partitions from the circulation into pulmonary secretions, with a lack of active circulating API, HNE's activity is increased, resulting in emphysema.[34,47]

1.7 Targeting PR3 in GPA

PR3 belongs to the chymotrypsin-like proteinase superfamily.[48] This group includes HNE and Cathepsin G, both of which are also stored in azurophilic granules alongside PR3 in neutrophils.[20,48] This class of proteinases can degrade extracellular matrix macromolecules such as elastin, fibronectin, laminin, vitronectin and type IV collagen.[48] In addition to its aforementioned intra-nuclear effects, PR3 can attack other nuclear substrates. These targets include the transcription factors nuclear factor-κB and SP1, and cytokines such as TNF-α, transforming growth factor-β1, and interleukin-1β.[20]

In GPA, when neutrophils are activated and degranulated, they do not only release PR3 but other contents as well, including HNE.[3] Due to their structural similarities, PR3 and HNE share the same natural inhibitor: API.[49] However, wild-type API is at a disadvantage at inhibiting PR3; it inhibits PR3 approximately 100 times less rapidly than HNE, with second order rate constant (k_2) values of $4.5x10^5$ and $6.5x10^7$ $M^{-1}s^{-1}$, respectively.[50,51] Therefore, with a decreased specificity towards PR3, and the abundant presence of the proteinase during neutrophil activation, wild-type API is not an ideal inhibitor. In other words, during degranulation HNE inactivation by API will be favoured, leaving excess amounts of PR3 that are released into the plasma uninhibited and free to cause endothelial damage. This project aimed to address this issue by exploiting the phenomenon seen with the API-R Pittsburgh variant, where mutations to the RCL of API changed its specificity towards thrombin, as mentioned earlier. This approach relied primarily upon phage display (see later sections).

HNE and PR3's sequences are 57% identical.[49] Both have similar primary cleavage substrate specificities.[52] Generally, elastases cleave after aliphatic amino acids such as valine, alanine and isoleucine. HNE has been shown to cleave substrates with all 3 amino acids in the P1 position.[52] However, PR3 has been shown to cleave after alanine better than HNE did. Furthermore, PR3 did not have any activity against substrates with isoleucine in the P1 position.[52] Based on published peptide phage display data, PR3 showed a preference for aromatic amino acids such as tryptophan both upstream and downstream of the cleavage site.[52] PR3 also cleaved substrates after aromatic amino acids at the P1 position, where HNE did not. Furthermore, both enzymes tolerated both

positively charged and negatively charged residues, upstream and downstream of the P1 position.[52] However, PR3 seemed to have lower activity to substrates with aromatic or negatively charged amino acids in the P1' position, suggesting that it does not cleave before aromatic residues. Overall, this shows that HNE does not cleave after aromatic residues, but PR3 does.[52] Because there are some differences in preference between the two proteinases, it is possible to contemplate the design or selection of an inhibitor with a higher specificity towards PR3 than HNE, to effectively target PR3 in GPA.

1.8 Previous Anti-PR3 Strategies

There is a need for a specific PR3 inhibitor that does not cause any immunological side effects. Investigators have produced recombinant PR3 inhibitor candidates by mutating their corresponding wild-type proteins.[52-55] Groutas et. al utilized a reactive site variant of α-1-antichymotrypsin (ACT) and substituted its P3-P3' residues with those from API. Although this variant showed inhibition of PR3, its second order rate constant of binding with PR3 (k_2 1.9 X 10^5 M^{-1} s^{-1}) was 5-fold lower than HNE (k_2 1.0 X 10^6 M^{-1} s^{-1}). Jegot et al. generated a variant of SERPINB1 (also known as leukocyte elastase inhibitor (LEI)), to inhibit PR3. They substituted the pentapeptide STADR for the natural AFTCM sequence at positions P4-P1' in the RCL of SERPINB1. This variant rapidly inhibited PR3 (k_2 of 1.4 X 10^7 M^{-1} s^{-1}) but was cleaved and inactivated by HNE without HNE inhibition.

Furthermore, small molecule inhibitors and mouse monoclonal antibodies with anti-PR3 function have also been generated.[56,57] Although there was some improved specificity for PR3, no previous anti-PR3 strategy produced sufficient specificity or

activity against PR3 with a sufficiently favourable toxicity/immunogenicity profile to move past the pre-clinical phase. This gap demonstrates the necessity of exploring the engineering of a viable PR3 inhibitor.

1.9 Benefits of Phage Display

As mentioned earlier, using serpins to inhibit PR3 could be a possible strategy to target this proteinase in GPA. Engineering a serpin by altering residues within its RCL could alter its specificity towards the proteinase.[31] Although there are no specific rules on how to engineer serpins, one way is to use phage display.[58] This system utilizes bacteriophages that express the mutant serpin fused to a bacteriophage capsid surface protein.[59] The recombinant phage DNA that codes for the mutant protein is stored safely within the capsid itself. Essentially, this technique allows for the expression of millions of variants of a serpin, which are hypervariable at a desired sequence of residues.[59] In the case of API, a recombinant library of API hypervariable at positions P7-P3 was previously fused to the T7Select capsid 10-3 protein (T7Select10) in our laboratory, and was used successfully to identify novel variants with increased rates of inhibition of thrombin.[60] The T7Select phage system allowed for the surface display expression of a full-length protein as large as 1200 amino acids, at 5-15 copies per phage, easily accommodating API's 394 amino acids.[59] The commercial system included an *Escherichia coli (E. coli)* strain pre-transformed with a plasmid designed to increase the number of coat proteins available, making phage production more rapid.[59] To screen the millions of variants, the randomized library was "biopanned" using thrombin.[60] The biopanning worked by using thrombin as "bait" to "fish" out the API variant that bound

with higher specificity to the protein.[59,60] This study used a P7-P3 hypervariable API library in which P1 was fixed as arginine (M358R),[60] and yielded two novel mutants with 2-fold increases in k_2 values for thrombin.[60] Validation of the phage display candidates required their re-expression as unfused recombinant API molecules, helping eliminate the possibility that lock-and-key inhibitors had inadvertently been created using an API scaffold.

Phage display has also been used to successfully express another serpin, PAI-1.[61] This proteinase inhibitor was expressed on the surface of M13 phage, which is a filamentous bacteriophage.[61,62] The formation of a serpin-enzyme complex by phage-displayed PAI-1 was confirmed, and its specific function was studied.[61,63] The developed PAI-1 libraries yielded mutants with increased stability and resistance to the latent or inactive conformation.[63]

2 Hypothesis

The hypothesis that was tested in this work was that altering the API RCL at residues P4-P1' inclusive would increase its specificity for, and activity against, PR3. These residues were chosen as they were previously mutated in SERPINB1, which resulted in a rapid inhibitor of PR3 (k_2=1.4x10^7).[54] However, as mentioned earlier, this variant was inactivated by HNE.[54]

3 Specific Objectives of the Project

The specific objectives of this project were as follows:

i. To create an API expression library hypervariable between RCL residues P4-P1' (API-P4P1') inclusive using DNA manipulation and cloning techniques;

ii. To biopan a previously generated API-P2P1 hypervariable phage library against PR3 to determine the feasibility of screening a larger hypervariable library (P4-P1');
iii. To insert the hypervariable API-P4P1' cDNA into T7Select10 phage;
iv. To perform a positive biopan using the API-P4P1' library against PR3 to determine optimal residues for PR3 specificity and deep sequence the lysate of each biopanning round;
v. To express and purify API-DA from the positive API-P4P1' biopan in a bacterial expression system
vi. To functionally screen the lysate library generated from the 3rd round of positive biopanning using a microtiter plate assay to help randomize the selection of variants;
    a. Generate and purify the high-binding variants, if different from the obtained deep sequencing results;
vii. To characterize the selected variants kinetically against PR3 to determine the best inhibitor of PR3.

4 Methods

4.1 Biopanning API-P2P1 Hypervariable Phage Library

4.1.1 Amplifying API-P2P1 Phage Library Glycerol Stock via Liquid Lysate Amplification

6 mL of overnight BLT5403 (Novagen T7Select) *E. coli* bacterial culture was diluted (1:50 dilution) in 50mL of Luria Broth (LB) and ampicillin (LB+AMP

100µg/mL) and shaken at 225 rpm at 37ºC in an environmental shaker until an OD_{600} of 0.677 was reached. The number of bacterial cells were then calculated using the following formula:

$$OD_{600} \text{ x} \frac{2\text{x}10^8}{0.5} \text{ x } 100 = \text{\# of cells}$$

The culture was then infected with a previously made API-P2P1 phage library[60] (T7Select103b phage supplied by Novagen) at a multiplicity of infection (MOI) of 0.001-0.01 (i.e. 100-1000 cells per plaque forming unit (pfu) of phage). This ratio allowed for a substantial excess of bacterial cells to avoid rapid lysis of all the host cells in solution. The infected BLT5403 culture was then allowed to shake at 225 rotations per minute (rpm) at 37ºC for approximately 2-3 hours until lysis of bacterial cells was observed. The solution was then centrifuged at 8000xg at 4ºC for 10 minutes. The supernatant containing the amplified phage lysate was harvested and stored at 4ºC.

4.1.2 Plaque Assay to Determine API-P2P1 Amplified Phage Lysate Titer

This protocol was based on the Novagen T7Select system manual.[64] The host bacterial strain was BLT5403 *E. coli*. Serial dilutions of the amplified lysate (produced as in Section 4.1.1) were made in LB. The dilutions reached up to $1/10^8$ of lysate to LB. 250µL of the host strain (OD_{600} ~0.5) was added to three 4mL sterile tubes marked A, B and C. Dilutions $1/10^6$, $1/10^7$ and $1/10^8$ of the lysate were added to tubes A, B and C respectively. Three dilutions were used in case the phage titer was too low to form plaques at higher dilutions. 3mL of melted top agarose was added to each tube. The tubes were gently shaken to mix the different components and then poured onto pre-warmed (37ºC) LB+AMP agar plates. Once the top agarose hardened, the plates were inverted and

stored at room temperature (RT) overnight to allow for plaque formation. This assay resulted in a lawn of bacteria in which clear phage plaques formed. The phage titer was then calculated by counting the amount of plaques on one of the plates and using the equation:

$$\#\text{ of plaques x dilution factor x } 10 = \text{ titer in pfu/mL}$$

4.1.3 Plaque Lift of API-P2P1 Amplified Lysate Plaque Assay

An immunoblotted plaque lift was done on the API-P2P1 amplified lysate plaque assay to ensure that the phage were producing API. This protocol was based on the Novagen T7Select system manual.[64] Plaque assay LB+agar plates expressing phage were chilled for 1 hour at 4^{o}C prior to use to reduce the tendency of top agarose to stick to nitrocellulose membrane. The membrane was first placed on the plate to cover it entirely. After 1 minute of contact, the membrane was peeled off and inverted on a plastic wrap to air dry for 10-20 minutes. The membrane was then soaked in blocking buffer [3% bovine serum albumin (BSA) in 1X Tris-buffered saline containing Tween 20 (TBST)] for 30 minutes with gentle rocking, to block non-specific binding of antibody. The blocking solution was discarded. Affinity purified sheep anti-human horse radish peroxidase (HRP)-conjugated anti-antitrypsin immunoglobulin G (IgG) polyclonal antibody (Affinity Biologicals) was then diluted in blocking buffer at 1/5000. This solution was then added to the membrane for 30 minutes with gentle rocking. After discarding the antibody solution, the membrane was washed 3 times for 5 minutes with 25 mL of 1X TBST. After the final wash, developing solution (5mg 3,3'diaminobenzidine, 200µL of 1% cobalt chloride, 9.8mL of 1X phosphate buffered saline (PBS) and 10 µL of 30% hydrogen

peroxide in 10mL solution) was used to visualize plaques containing anti-antitrypsin-reactive antigen. The number of plaques was then compared to that generated in the corresponding plaque assay to ensure the expression of API on the surface of the phages being used.

4.1.4 Biopanning the API-P2P1 Phage Lysate with PR3

$1x10^9$ pfu phage lysate was added to 3% BSA in 1X PBS in a total volume of 1mL. 2nM final concentration of PR3 was added to the experimental (EXP) condition and the equivalent volume of 3% BSA in 1X PBS was added to the negative (NEG) control. The solutions were incubated at 37°C for 30 minutes. To block any unbound PR3, 1µL of 100mM phenylmethylsulfonyl fluoride (PMSF) was added to both solutions. 1µg of affinity purified rabbit anti-human biotinylated anti-PR3 polyclonal IgG antibody was also added to both conditions. The reactions were mixed at RT for 30 minutes with end-over-end rotation. 50µL of resuspended streptavidin-coated magnetic beads (Dynabeads) was added to both reactions and mixed at RT for 30 minutes with rotation. The phage-serpin-proteinase-antibody-bead complexes (Figure 2) were pulled down using a magnetic stand for 2 minutes and the supernatant was discarded. The complexes were then washed with PBS+1% Triton-X-100 for 5 minutes with rotation. The wash step was repeated 10 times and the washed beads were transferred to a fresh tube after every second wash. After the final wash, the complexes were resuspended with 0.5mL PBS. The EXP beads were inoculated with 35mL of BLT5403 cells grown in LB+AMP to an OD_{600} of 0.8. The NEG beads were inoculated in the same volume of BLT5403 cells for the first round of biopanning, or in 15mL of cell culture in the consequent steps due to

low phage titer (based on plaque assays done after each round of selection). The infected bacterial cultures were then shaken at 37ºC until lysis was visible after approximately 2-3 hours. The solutions were then centrifuged, and the lysates were titered via plaque assay as described above. The new lysates were then used for the next round of biopanning. The biopanning procedure was repeated for 5 rounds, with plaque assays performed after each round to determine the phage titer. The NEG lysate was amplified via liquid lysate amplification after rounds 2 and 4, due to the production of a low phage titer. The original lysate and the 5th round lysates from both the EXP and NEG were then subjected to Next Generation Sequencing (NGS), also called deep-sequenced, for analysis. The biopanning procedure is shown in Figure 3.

Figure 2: Phage-Serpin Complex.

Illustration of the phage-serpin-proteinase-antibody-bead complex used during the biopanning protocol.[59]

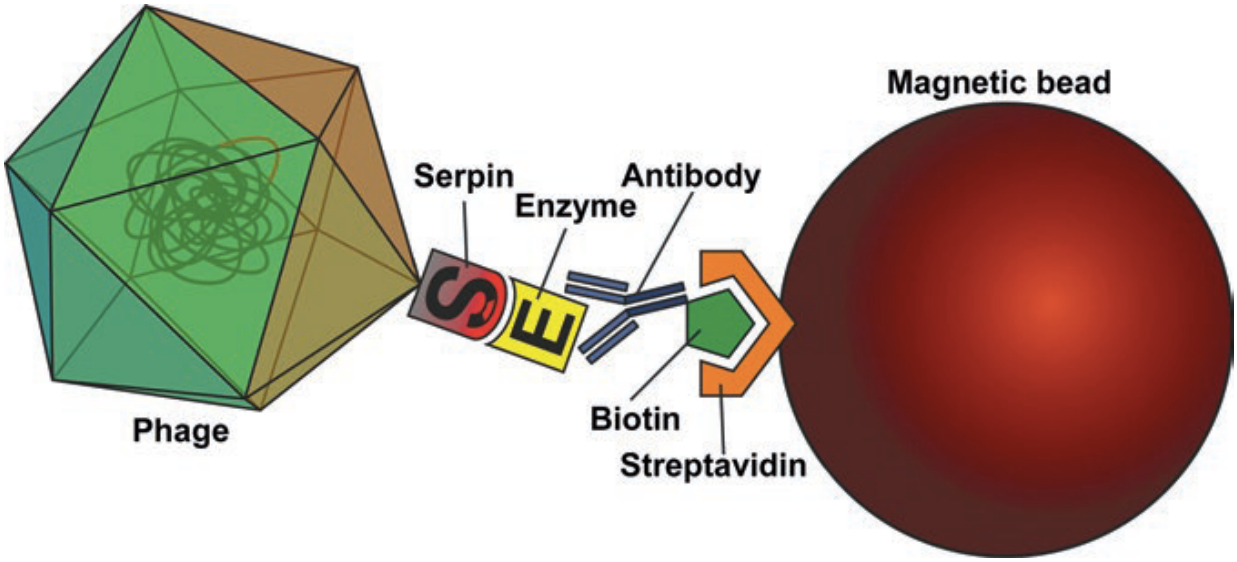
Magnetic bead
Serpin
Enzyme
Antibody
Phage
Biotin
Streptavidin

Figure 3. Biopanning Procedure (schematic diagram).

The process begins by amplifying the API-expressing phage in bacterial culture. The screening complex is then assembled by adding PR3 (green boxes) (step 1), biotinylated antibody (purple "Y", step 2) and streptavidin-coated magnetic beads (yellow "S" and red circles, step 3). This phage-PR3-antibody-streptavidin-bead complex is then pulled down using a magnet and washed to eliminate non-specifically bound phage and PR3 (step 4). Finally, the resultant selected phage population is used to infect a new bacterial culture by direct inoculation (step 5). This lysate is then amplified and the new phage lysate becomes the starting material for the next round. We performed a total of 5 rounds of biopanning.[60]

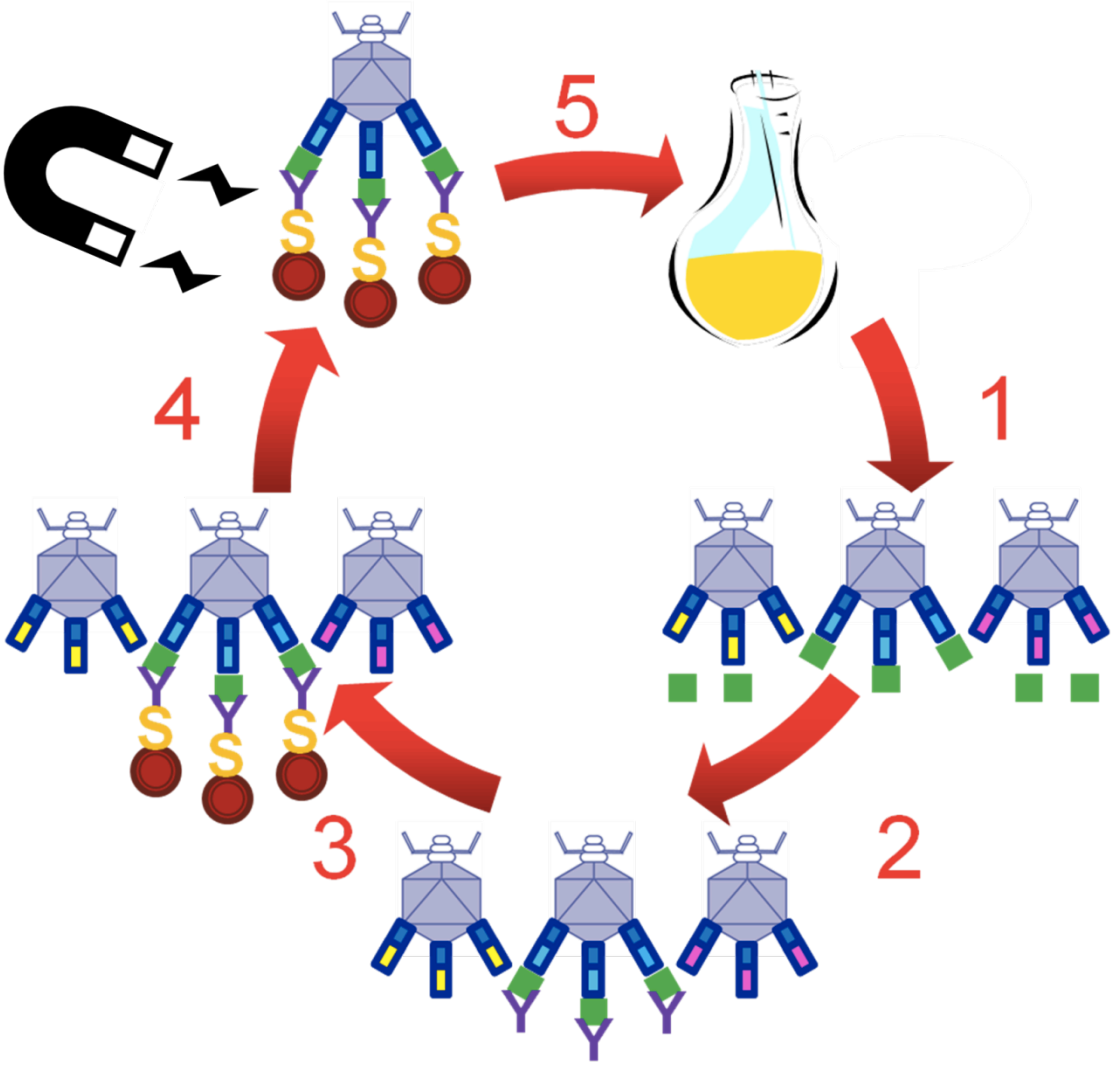
5
1
2
3
4
S
S
S
S
S
S

4.2 Preparing Phage Library for Deep Sequencing

To prepare the selected or non-selected phage libraries for deep sequencing, they were first amplified through polymerase chain reaction (PCR), as per the Thermo Scientific Phusion High-Fidelity DNA Polymerase manual. The sequences for the sense oligodeoxyribonucleotide primer (S-Phage-API) and anti-sense primer (AS-Phage-API) can be found in Table 1. Each primer had a different tag to distinguish the biopanned libraries during the deep sequencing protocol. Approximately 5 x10^7 pfu of phage lysate was used to provide the template DNA for the PCR reaction. Samples were then sent to the Mobix Lab at McMaster University for deep-sequencing (Illumina NGS). The samples were analyzed in parallel with samples from other labs, with all the samples loaded on the same plate, to minimize cost. The coverage or "read-out" for our samples was 1% (i.e. the number of sequences detected comprised 1% of the total sequences on the entire plate).

4.3 Cloning API-P4P1'

To produce API-P4P1', an oligonucleotide encoding the API RCL was used. In this sequence, the nucleic acid bases that coded for residues P4 to P1' were randomized as shown in Table 1.

Cloning protocols were employed to produce API-P4P1' inserted into a pUC19 plasmid vector, which had EcoRI and HindIII restriction sites that corresponded to T7Select103b phage vector arms. The template used for the PCR was pBAD-API-R (M358R)[46] with sense PmlI and antisense P4P1' random oligonucleotides (Table 1). The PCR protocol was as done as per the Thermo Scientific Phusion High-Fidelity DNA

Polymerase manual. The PCR product was then purified using a Thermo Scientific GeneJET PCR clean-up kit.

Table 1: Oligonucleotides Used in PCR Experiments.

'N' indicates any nucleic acid base.

Sense PmlI	5’ CAAGGACACCGAGGAAGAGGACTT 3’
Antisense P4P1’ random	5’ CTTGACCTCAGGTGGGATNNNNNNNNNNNNNNCTCTAAAAACATGGCCCCAGC 3’
S-API-N-TERM	5’ GAGGATCCCCAGGGAGATGCTGCCCAGAAGACAGATACATCC 3’
AS-API-DA	5’ CTTGACCTCAGGTGGGATAGAAGCGTCTATGGCCTCTAAAAACATGGC 3’
S-Phage-API	5’ GATCCGAATTCAGAGGATCCCCAGGGAGATGC 3’
AS-Phage-API	5’ GCTAAGCTTCATTTTTGGGTGGGATTCACCAC 3’

4.3.1 Restriction Enzyme Digest of PCR Product and Vector Plasmid

The pBAD-API-P4P1' PCR product was digested using Thermo Scientific FastDigest BamHI (10U/µL) and Bsu361 (10U/µL), following the manufacturer's guidelines. This digestion produced the 1082 base pair (bp) insert that contained the randomized P4-P1' RCL sequence. The digestion reaction was then electrophoresed on a 1% agarose gel and the band of interest was excised and purified using a Thermo Scientific GeneJet gel extraction kit.

The digestion of the pUC19-API-P2P1 plasmid that would provide the vector for the subsequent ligation reaction was done in the same way as described for the above PCR product. However, this digestion included the addition of CIAP (1U/µL), an alkaline phosphatase. This manipulation dephosphorylated the 5' ends of the vector strand to prevent plasmid self-recircularization of any single-cut plasmids. These reactions generated a 2744bp pUC19-API vector preparation.

4.3.2 Ligation of API-P4P1' Insert and pUC19-API Vector

The insert and vector fragments were quantified using a Nanodrop spectrophotometer. The ligation reaction was set up using 10X T4 DNA ligase buffer and 1µL of T4 DNA ligase 5U/µL (Thermo Scientific). The amount of insert needed was calculated using the equation:

$$ng\ insert = ng\ vector \times \frac{size\ of\ insert\ in\ base\ pairs}{size\ of\ vector\ in\ base\ pairs} \times desired\ molar\ excess$$

A 3:1 molar excess of insert to vector was used in a 20µL reaction volume. The reaction was incubated at RT for 1 hour. A negative control reaction was also carried out, one that followed all the same parameters but did not include the insert fragment.

4.3.3 Transforming pUC19-API-P4P1' into E. coli DH5α

The pUC19-API-P4P1' ligation product and the negative control from the ligation reactions were separately transformed into *E. coli* DH5α competent cells. 50µL of cells and 5µL of ligation product (25% of total ligation mixture) or water were employed, respectively. The reactions were incubated on ice for 15 minutes, then heat shocked at 37°C for 20 seconds, and then returned on ice for another 2 minutes. 1mL of RT LB was added to each reaction and the suspension was then shaken at 37°C for 1 hour. The tubes were then centrifuged at maximum speed (14000Xg) for 1 minute and the supernatant was partially decanted. The cells were resuspended and plated on LB+AMP agar plates. The plates were incubated overnight at 37°C. This transformation was done to ensure that there was a sufficiently low background in order to transform the remainder of the ligation reaction for mass plasmid propagation (see next section). Furthermore, this allowed for an initial assessment of the depth of the library, which was determined through counting the number of colonies that grew on the plate, and back-calculating to determine the approximate number of sequence variants in the ligation mixture. Selected colonies were spot-checked by DNA sequencing to ensure the randomization of P4-P1' RCL sequence. Each colony was grown in 6mL LB+AMP culture and the plasmid was extracted using Thermo Scientific GeneJET plasmid miniprep kit.

4.3.3.1 Mass Plasmid Propagation

The remaining experimental ligation reaction was transformed as described above. However, since 15µL of DNA was used, the amount of DH5α competent cells was scaled up to 150µL. The entire transformation product was grown in 200mL of LB+AMP

overnight at 37°C with shaking, instead of being poured on agar plates. Plasmid DNA was then extracted from the cells using the Thermo Scientific GeneJET plasmid midiprep kit and the purified pUC19-API-P4P1' plasmid DNA was quantified using Nanodrop spectrophotometer.

4.4 Inserting API-P4P1' into T7Select Vector

The pUC19-API-P4P1' plasmid was digested using restriction enzymes EcoRI and HindIII as these correspond with the ends of the T7Select10 vector arms. The digestion protocol was the same as the one described above, with 5µg of plasmid digested. The insert fragment generated, which encoded was full length API-P4P1', was ligated with the T7Select10 vector arms following the protocol described in the Novagen T7Select system manual.[64] In this reaction, 0.027pmol of insert DNA and 0.02pmol of vector arms were added for a ratio of 1.35:1 of insert to vector.

4.5 In Vitro Packaging of Ligation Reaction

The packaging of the T7Select103b-API-P4P1' DNA was done following the protocol outlined in the Novagen T7Select system manual.[64] 5µL of API-Phage ligation reaction was added to 25µL of T7Select packaging extract. They were stirred gently to mix and incubated at RT for 2 hours. The reaction was stopped by adding 270µL of sterile LB.

The *in vitro* packaging phage product was titered by plaque assay and amplified via liquid lysate amplification and a glycerol stock was made from the lysate. The titer of the amplified library was also determined through plaque assay, and an immunoblotted plaque lift was also done to ensure that the phages were API producing. This lysate was

also used for the subsequent biopanning protocol of the API-P4P1' phage library with PR3.

4.6 Biopanning API-P4P1' Phage Library with PR3.

The biopanning of the API-P4P1' phage library followed the same approach as described in section 4.1.4, except that after the 2nd round of biopanning, the washed EXP phage-serpin-proteinase-antibody-bead complex solution was inoculated into 25mL of BLT5403 bacterial culture instead of 35mL. This was done to ensure a high enough titer for subsequent rounds of biopanning. After 5 rounds of biopanning, the final lysate from the EXP and NEG reactions were deep-sequenced for analysis.

4.7 Cloning pBAD-API-DA

The PCR protocol for generating pBAD-API-DA plasmid was similar to that used in Section 4.3 (where API-DA is API P357D/M358A). However, different sense (S-API-N-TERM) and antisense (AS-API-DA) primers were used. The primers' sequences can be found in Table 1.

4.7.1 Inserting API-DA into pGEX Bacterial Vector

The PCR product pBAD-API-DA and the vector plasmid pGEX-API-R were digested using restriction enzymes to produce a pGEX-API-DA plasmid, which was tagged with both hexahistidine and glutathione-S-transferase (GST) segments for protein purification purposes. The digestion procedure was similar to that employed in Section 4.3.1. The enzymes used in this experiment were Bsu361 and Knp21. The resulting insert and vector fragments were ligated as described in Section 4.3.2. The ligation product was then

transformed (as discussed in Section 4.3.3) into *E. coli* BL21 competent cells for protein expression.

4.8 Recombinant Histidine-Tagged and Glutathione-S-Transferase Fusion Protein Expression in Bacterial Expression System

The following protocol was applied to express all the recombinant variants of API. A glycerol stock of *E. coli* BL21 cells expressing only one variant of API was scraped using a sterile tooth pick and added to LB+AMP (100µg/mL) solution and the bacterial cells were grown overnight at 37ºC while shaking at 225rpm. The next morning, the overnight culture was added to 1L LB+AMP (100µg/mL) in a 1/50 dilution. The culture was then allowed to grow to an $O.D._{600}$ of ~0.5 at 225rpm and 37ºC. Once the desired O.D. was reached, protein expression was induced using isopropyl β-d-1-thiogalactopyranoside (IPTG) at a final concentration of 0.1mM. After 4 hours of induction at 225rpm and 37ºC, the bacterial cells were harvested by centrifugation at 6,000 rpm at 4ºC. The supernatant was discarded, and the pellets stored at -20ºC. The volume of growth media and amount of the other reagents were scaled up or down as needed, to generate more, or less protein.

4.9 Recombinant Histidine-Tagged and Glutathione-S-Transferase Fusion Protein Purification

The following protocol was applied to purify all recombinant API variants. Bacterial pellets from a 1L culture were resuspended with 20mL PBS, with one Complete Protease Inhibitor Cocktail tablet (Roche) added/1L culture. The solution was then placed on ice and sonicated for 3 minutes at an amplitude of 30% with 5 seconds on/5 seconds off pulses using Sonics Vibra Cell Sonicator model VCX500. The sonicated cells were then

placed in a centrifugation tube with Titron X-100 at a 1% final concentration. The solution was rocked at RT for 15 minutes. It was then centrifuged at 12,000rpm for 30 minutes at 4ºC to pellet the cell debris. The cell lysate was then added to 1.5mL glutathione agarose resin (equilibrated with PBS) and allowed to batch-bind through the GST-fusion protein for 40 minutes. The glutathione agarose beads were stored in a 1:1 slurry of 30% ethanol to agarose beads solution, hence the need for an equilibration step. The agarose beads were then poured into a purification column and the flow-through was collected. The resin was then washed with 10 column volumes of PBS followed by 10mL of HRV3C Cleavage Protease buffer (Thermo Scientific). The wash buffers were also collected. 20µL of HRV3C Cleavage Protease (2U/µL) in 3mL of cleavage buffer were added to the resin. The resin was then rocked at 4ºC overnight to cleave the GST-fusion protein from the recombinant API variants.

The next morning, the unbound fraction of the column was collected and added to a packed volume 1.5mL of nickel chelate affinity (Ni-NTA agarose) resin (equilibrated with PBS) as an additional purification step. These beads were also stored in the same conditions as the aforementioned glutathione agarose beads. The flow-through was collected and the resin was washed with 20mL of PBS and 20mL of 50mM sodium phosphate/300mM NaCl/20mM imidazole/pH 8. After collecting the wash solutions, the histidine-tagged recombinant protein was eluted from the column with 50mM sodium phosphate/300mM NaCl/250mM imidazole/pH 8 and collected using a fraction collector. Samples of the elution fractions were then visualized on a 10% sodium dodecyl sulfate-polyacrylamide gel electrophoresis (SDS-PAGE) gel. The fractions showing the presence

of protein were then pooled and dialyzed overnight into PBS at 4ºC. The dialyzed solution was then concentrated through centrifugation, aliquoted and stored at -80ºC. The glutathione-sepharose column was also eluted with 2mM glutathione, and the fractions were visualized on a 10% SDS-PAGE gel.

4.10 Bradford Assay to Quantify Purified Recombinant Protein

BSA was used to create a protein standard for this assay. Eight dilutions of 2mg/mL BSA ranging from 0.1-1.0mg/mL (in PBS) were made. Undiluted, 1 in 2 and 1 in 5 diluted samples of purified protein were also created (in PBS). 5µL of each standard dilution, sample and blanks composed of only buffer were added in duplicate to a 96 well microtiter plate. 200µL of Coomassie Plus Protein Assay Reagent (Thermo Scientific) was added to each well. The plate was read using a BioTek EL808 plate reader.

4.11 ELISA Protocol for Recombinant Protein Quantification

The purified recombinant proteins were first quantified using Bradford assay. The estimated concentrations were then used to dilute the protein to lie within the standard curve used for the ELISA protocol. The procedure was done as per the Matched-Pair Antibody Set for ELISA of Human α1-Antitrypsin Antigen manufacturer's instructions (Affinity Biologicals). Plasma-derived API-wild-type (PD-API-WT) was used to generate the standard curve for all ELISA experiments. Anti-API capture antibody was diluted in coating buffer (50mM carbonate pH 9.6) at 1/100 dilution. 100µL of capture antibody was used to coat each well in a microtiter well plate and incubated at 4ºC overnight. The next day, the coating solution was discarded, and the wells washed once with PBS-T (PBS with Tween-20 0.1% v/v). The plate was then banged on a stack of paper towels to

eliminate any moisture in the wells. 200µL of blocking buffer (PBS with BSA at 1% v/v) were added to each well and incubated at RT for 1 hour. Each API sample was prepared at 3 dilutions to fall within the standard curve. After blocking the wells, the blocking buffer was discarded, and the wells washed twice with PBS-T. The samples and standard were then loaded in duplicate using 100µL per well and incubated for 1 hour at RT. The solutions were then discarded, and wells washed 5 times with PBS-T. Anti-API detecting antibody was diluted in blocking buffer at 1/100 dilution and added to each well using 100µL of solution. The detecting antibody was incubated for 1 hour at RT. The antibody solution was then discarded, and the wells washed 5 times with PBS-T. 100µL of TMB developing solution (Thermo Scientific) was then added to each well and allowed to incubate for 10-30 minutes. Wells with a positive signal displayed blue colouration. The reaction was stopped with 2M sulfuric acid. The plate was then read using a Biotek ELx808 spectrometer at 450nm.

4.12 Mass Lysate Screen using Round 3 Phage Display Lysate

This screen was done in addition to the phage-display screen to detect any other possible high-binding candidates in addition to API-DA. A small volume of Round 3 phage lysate (~25 µL, titer $6x10^{11}$pfu/µL) selected with PR3 was scraped from the surface of a frozen aliquot using a sterile toothpick, and added to 50µL of autoclaved ddH_2O. The phage solution was heated at 95^{o}C to lyse any bacteria in the sample. The 3rd Round lysate was then used as the template for PCR reactions to amplify the randomized RCL DNA segment. The primers used were S-Phage-API and AS-Phage-API (Table 1). The PCR product and a pBAD-API-R plasmid DNA sample were digested using the

restriction enzymes EcoNI and HindIII as described earlier. The insert (RCL fragment from PCR) and vector (pBAD from pBAD-API-R plasmid) were ligated as mentioned in previous sections. The resultant plasmid library was then transformed into *E. coli* Top10 competent cells. Additionally, pBAD-API-WT (positive control in the screen), pBAD-API-R and pBAD empty vector (negative controls) plasmids were also transformed into Top10 competent cells.

The mass lysate screen was set up similarly to an ELISA protocol. Microtiter plate wells were coated with 100µL of PR3 (1µg/mL) diluted in PBS overnight at 4°C. For each experiment, 16 colonies from the Round 3 library transformation plate and 2 colonies from each of API-WT, API-R and empty vector were picked and grown overnight in LB+AMP (100µg/mL) at 225rpm and 37°C. Each of the 16 colonies were dotted on a gridded LB+agar plate and allowed to grow at 37°C overnight. The next morning, arabinose (0.002% final concentration) was added to the bacterial cultures to induce protein production for 3 hours at 225rpm and 37°C. 2mL from each sample was collected and centrifuged at maximum speed for 2 minutes in a table-top centrifuge. The supernatant was discarded, and the bacterial pellets were resuspended in 0.5mL PBS. Each sample was then sonicated for 10 seconds. The samples were then centrifuged for 20 minutes at maximum speed to pellet the cell debris. Prior to sonication, the PR3 coating solution was discarded and the PR3-coated wells were washed once with PBS-T, then blocked with 5% milk powder in PBS-T for 1 hour at RT. The blocking solution was then discarded, and the wells were washed 5 times with PBS-T. The lysate supernatants were then added in duplicate along with a blank solution of only PBS, and incubated for 1

hour at RT. The lysate supernatants were then discarded, and the wells were washed 5 times with PBS-T. HRP-conjugated anti-antitrypsin antibody (same antibody used in section 4.1.3) was diluted 1/5000 in blocking solution and added to each well and incubated for 1 hour at RT. The antibody solution was then discarded, and wells washed as above. TMB developing solution (Thermo Scientific) was then added to each well for colour development. This reaction was then stopped using 2M sulfuric acid. The plates were read using a Biotek ELx808 spectrometer at 450nm.

This procedure was repeated twice for a total of 32 screened colonies. The wells showing positive results were matched with their colonies on the gridded plates. Those colonies were then picked, grown in LB+AMP (100µg/mL) and their plasmid DNA was extracted using the Thermo Scientific GeneJET plasmid miniprep kit. The resulting plasmid DNA samples were then sequenced for RCL sequence determination. In some experiments, purified coagulation fXIa[60] was substituted for PR3 (with 100µL of 0.1µg/mL purified fXIa used to coat the wells) and purified recombinant API-WT, API-R, or API-DA at 2.5 – 5.0 µg/mL was substituted for bacterial lysates. In others, lysates from 2mL of cell culture were substituted for lysates from 1mL of cell culture.

4.13 Serpin-Proteinase 3 Gel-Based Complexing Assay

An SDS-PAGE gel-based complexing assay was used to determine if the novel API variants formed a complex with PR3, with API-WT serving as the positive control. The experimental procedure was the same for all API variants. The variants and PR3 were reacted at 3 different molar concentration ratios 10:1, 5:1 and 1.5:1 (API:PR3) with 1µM PR3 used for all ratios. Each reaction was done by adding the appropriate concentration

of API, based on the stock concentrations determined through ELISA, and PR3, based on the concentration provided by the manufacturer. Each reaction was allowed to proceed for 5 minutes at 37°C and was stopped by adding SDS-PAGE loading dye. The reaction mixtures were then loaded onto a SDS-PAGE gel and visualized through traditional Coomasie Brilliant Blue staining and destaining techniques.[65]

Through this experiment, optimal molar concentrations of API were determined for subsequent kinetic analyses.

4.14 Unsuccessful Kinetic Characterization of API-PR3 Binding using FRET Substrate

To determine the k_2 of API to PR3 binding, a PR3 specific fluorescence resonance energy transfer (FRET) substrate developed by Korkmaz et al. was employed.[66] The method used to calculate the second order rate constants was based on work done by Beatty et. al and adapted by Korkmaz et al. and Sinden et al.[50,51,67] Equimolar amounts of PR3 and API (1nM each) were mixed in a 150µL reaction volume in black opaque microtiter well plates. Each protein was diluted in NSP assay buffer [50mM Hepes, pH 7.4, 150mM NaCl, 0.05% Igepal CA-630 (v/v)]. Residual PR3 activity at 1 to 5 minutes of incubation was measured by stopping the reaction with 3µL of the PR3 specific FRET substrate Abz-Val-Ala-Asp-Nva-Arg-Asp-Arg-Gln-EDDnp at a concentration of 1mM. The change in fluorescence was measured every 2 minutes for 40 minutes (excitation 340nm and emission 460nm) using the Thermo Fluroskan Ascent fluorospectrometer. The k_2 value was then calculated by plotting the inverse of PR3 activity at each time point

versus time. From the linear portion of the slope, the half-life ($t^{1/2}$) of the reaction was calculated using the formula:

$$t^{\frac{1}{2}} = \text{y}\frac{\text{intercept}}{\text{slope}}$$

The k_2 value was then calculated using the following equation:

$$k_2 = \text{Concentration of PR3 x } t^{1/2}$$

4.15 Serpin-Proteinase 3 Gel-Based Kinetic Analysis

Gel-based kinetic analysis was done for the novel API variants, with API-WT being the main comparator, to determine the second order rate constant (k_2) for the API-PR3 interaction. This analysis was done for one of the novel API variants (API-N, i.e. API S359N) and not the other (API-DA) due to the suspension of graduate research activities caused by the novel coronavirus (COVID-19) pandemic.

This reaction was done under pseudo-first order conditions (10:1 API to PR3 molar ratio) at 37°C. Under these conditions, the change in concentration of API becomes negligible, making the reaction dependent on the concentration of PR3 only. The reaction was allowed to progress for 5 minutes with 20µL aliquots taken out of the reaction tube and added to SDS-PAGE loading dye. This allowed for the collection of reaction samples at 1-minute intervals. The samples were then loaded onto an SDS-PAGE gel and analyzed by immunoblotting using HRP-conjugated anti-API antibody. Each blot was imaged using a Bio-Rad Gel Doc XR instrument. Once imaged, the complex band intensities were quantified using the QuantityOne companion software (Bio-Rad). The intensities were measured through the "band intensity" function in the QuantitytOne software. Moreover, only blots with API-N-PR3 complex bands were also measured through the

"band volume" function of the software (due to COVID-19). Each API variant was tested 5 times (n=5) for subsequent statistical analysis.

4.16 Standard Curve Generation for Gel-Based Kinetic Assay

To calibrate the immunoblots produced by the gel-based kinetic analysis of API-PR3 binding, a standard curve of known concentrations of API was generated. However, only one calibration experiment was completed for the recombinant API variants, due to COVID-19 closures.

The API-PR3 bands could reach a theoretical maximum concentration of 1μM, as that corresponded to the maximum amount of PR3 used in the gel-based kinetic assay. Therefore, recombinant API-N was diluted to 2, 1, 0.5, 0.25, 0.125 and 0.0625μM concentrations. Aliquots of these dilutions were analyzed by SDS-PAGE. A parallel immunoblot was also generated, as described in previous sections. This blot featured bands from an API-N dilution series between 0.1 to 1μM of API-N. The calibration blot was then imaged using a Bio-Rad Gel Doc XR. The bands were quantified through the "band volume" function in the QuantityOne software. Due to COVID-19 restrictions, only API-N blots were measured through the same modality. Thus, the standard curve could not be used to calibrate the API-WT-PR3 complex bands.

4.17 SDS-PAGE Electrophoresis

10% SDS-PAGE gels were used to perform all electrophoresis protocols. 20μL of protein samples were mixed with 8μL of 4X SDS-PAGE loading dye. The mixture was then heated at 95^{o}C for 2 minutes. 20μL of the boiled solution was then loaded onto the gel. The samples were electrophoresed using a Mini-PROTEAN Tetra Vertical

Electrophoresis Cell (Bio-Rad) for 30-35 minutes. The resulting gels were either stained and destained for analysis (see previous sections) or underwent immunoblotting.

4.18 Immunoblot Protocol

The following protocol was applied to all immunoblots done in this project. Electrophoresed SDS-PAGE gels were transferred to a nitrocellulose membrane using iBlot Gel Transfer Stacks and an iBlot machine as per the manufacturer's instructions (Thermo Scientific). The membrane was incubated for 1 hour in 5% milk-TBST while rocking at RT. HRP-conjugated anti-antitrypsin antibody (same antibody used in section 4.1.3) was diluted 1/5000 in 10mL of 5% milk-TBST and added to the membrane for 1 hour with rocking at RT. After discarding the antibody solution, the membrane was washed 3 times for 5 minutes with 25 mL of 1X TBST. After the final wash, developing solution (5mg 3,3'diaminobenzidine, 200µL of 1% cobalt chloride, 9.8mL of 1X PBS and 10µL of 30% hydrogen peroxide in 10mL solution) was used to visualize the reactive bands. The immunoblots were then imaged using a Bio-Rad Gel Doc XR instrument.

4.19 Statistical Analysis of Gel-Based Kinetic Assays

Statistical analysis was performed using the InStat software from GraphPad. The data was analyzed using an unpaired t-test.

5 Results

5.1 Assembly and Characterization of a Hypervariable API-P4P1' Library

5.1.1 Size of API-P4P1' Library

The first experimental priority of this project was to create an API expression library hypervariable between the P4 and P1' codons of the API RCL. The library was characterized by plating a portion of the ligation reaction as described in Section 4.3.3. The vector plus insert pUC19-API-P4P1' condition yielded 616 colonies versus only 23 in the pUC19 vector only negative control. This finding suggested that the library contained ~2372 independent clones ([616 – 23] X 4), since only 25% of the ligation reaction was plated.

Eight colonies were picked at random from the plated cells transformed with the plated vector plus insert ligation reaction, as a spot check on the diversity of the library. Not only did these plasmids contain differing DNA sequences (data not shown), they each encoded different API variants at the primary sequence level; the 8 colonies picked from the 616 colonies had different randomized P4-P1' RCL residues (Table 2). This observation indicated that the cloning protocol was successful in producing pUC19-API-P4P1', hypervariable at P4-P1' residues, and rendered even less likely the remote possibility that DNA encoding other API variants previously studied in the laboratory had contaminated any step of library construction.

Table 2: Spot-check DNA Sequencing Results of Randomly Selected pUC19-API-P4P1' Colonies.

DNA samples prepared from liquid cultures grown from these colonies were sequenced using the Sanger sequencing method. The wild-type residues at those positions are AIPMS. The sequence for colony D was inconclusive, likely due to two colonies being picked simultaneously in error. The dash in sequence G indicates a stop codon.

Colony	P4-P1’ Sequence
A	QTPQP
B	NPCRL
C	PRTSH
D	S ? ? ? ?
E	YPNSS
F	ILQKA
G	HYIN-
H	RDTRD

5.1.2 Verification of Expression of API-P4P1' Library

The cloning protocols used to produce pUC19-API-P4P1' plasmid library were employed solely in order to package the hypervariable API-P4P1' cDNA into the T7Select10 phage. To ensure that this library was in fact API producing, an immunoblotted plaque lift was performed on the plaque assay of the original lysate generated after packaging. The results showed 450 immunoreactive plaque signals, which corresponded to the same number of plaques on the plaque assay (Figure 4, lower panels). This observation indicated that the phages were API producing (Figure 4). The *in vitro* packaging phage product's titer was $3.0x10^7$ pfu/mL, which was within the manufacturer's recommended range for efficient packaging. The specificity of the immunoreactivity was suggested by the lack of staining on plaque lifts from control phage expressing a 15 amino acid "S-tag" provided by the T7Select system manufacturers (data not shown).

Figure 4: Plaque Assay and Plaque Lift of the API-P2P1 and API-P4P1' Phage Libraries.

The top two images correspond to the plaque assay (panel A) and plaque lift (panel B) of the API-P2P1 phage library. The blots on the nitrocellulose sheets in panel B correspond to the plaques in the top agarose in panel A. The results indicate that the plaques were API producing. Panels C and D show the same results but for the API-P4P1' phage library, where panel C is the plaque assay and panel D is the plaque lift.

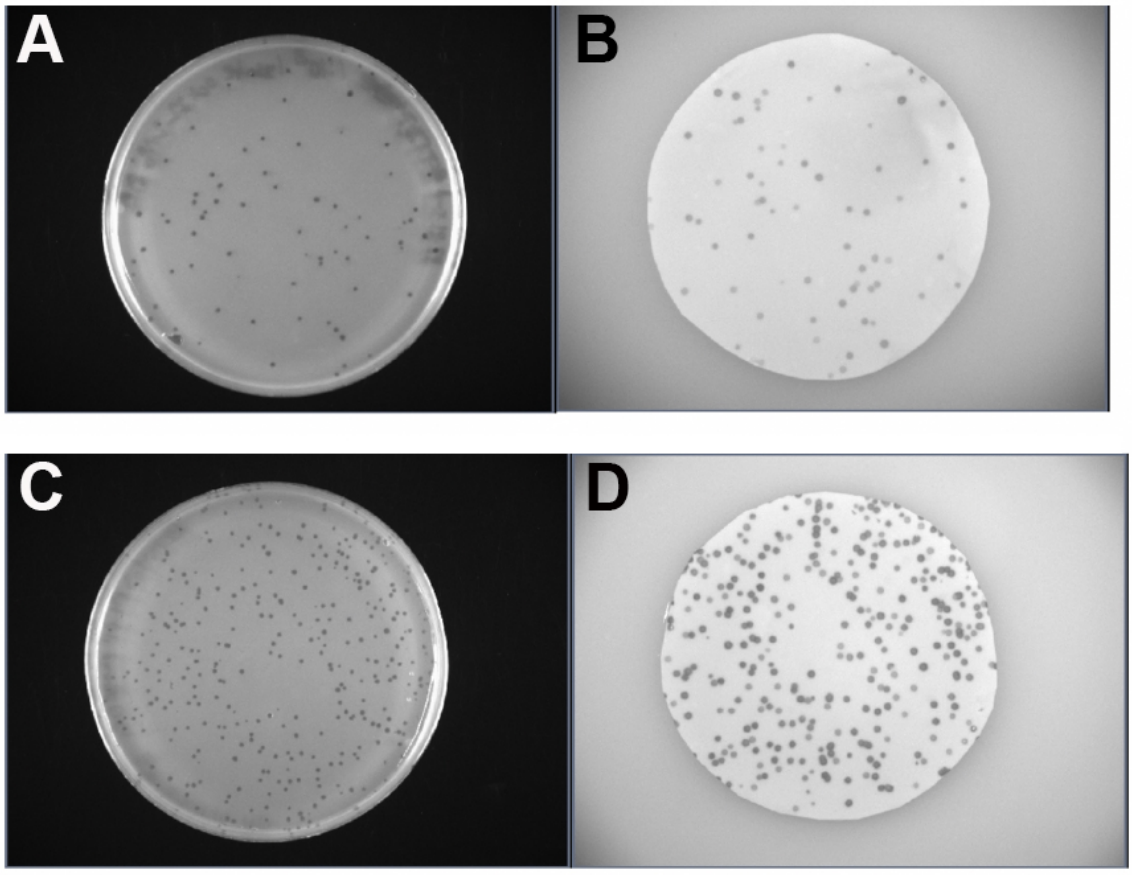
A
B
C
D

5.2 Screening an API-P2P1 Phage Library with PR3

After construction of the API-P4P1' library, it was decided to screen a previously constructed API-P2P1 phage library[60] with PR3 before employing the new library with its larger number of hypervariable codons.

5.2.1 Verification of Expression of the API-P2P1 Phage Library

Since the API-P2P1 phage library had been stored for >4 years since its last use, its ability to produce phage with immunoreactive API domains was verified. The immunoblotted plaque lift of the plaque assays for the API-P2P1 library showed 74 immunoreactive plaque signals, which corresponded to the number of plaques present in the plaque assay itself (Figure 4, top panels). This result demonstrated that the plaques were immunoreactive to anti-API antibody, therefore expressing API. This helped indicate that the library was eligible for biopanning as the correct serpin was expressed on the phage. The specificity of the immunoreactivity was suggested by the lack of staining on plaque lifts from control phage expressing a 15 amino acid "S-tag" provided by the T7Select system manufacturers (data not shown).

5.2.2 Biopanning the API-P2P1 Phage Library with PR3

Because the API-P2P1 biopanning experiments served as a trial run to determine the feasibility of using PR3 to screen API variants expressed by bacteriophages, only the unselected library and the 5th round screen were deep sequenced. In the unselected library, there were 4,593 different variants (based on the reads obtained from deep sequencing at the DNA level). The results from the 5th round screen showed the presence of 1,090 different API variants in the experimental (EXP, with PR3) condition and 525 in

the negative, or control (NEG, lacking PR3) condition. This reduction in the number of unique variants between the original and selected library indicated that PR3 was a feasible "bait" in the biopanning experiments.

The top 20 most abundant nucleotide sequences in the 5th PR3-selected biopanning round were chosen from the deep sequencing data and were translated and analysed using Clone Manager software. The most abundant P2-P1 encoded dipeptide in the EXP library was D357-A358 (API-DA) at 23,191 copies as well as the 5th most abundant at 6,572 copies (employing different codons from the other, major genotype). The second most abundant was S357-S358, followed by P357-M358 (wild-type API) with 11,369 and 10,126 copies respectively. API-DA was not abundant in the NEG condition, with only 1 copy. The relative difference in copies between API-DA and other variants indicated that the API-DA was a possible candidate for PR3 inhibition. Tables 3 and 4 show the top 20 P2-P1 sequences in the EXP and NEG conditions.

Table 3: Top 20 Most Abundant Variants in the 5th Round EXP Biopan.

The repeating variants were a result of different nucleic acid sequences expressing the same amino acid sequence. The numbers shown in this table represent the reads or copies of variants from the deep sequencing data. There was a total of 1,090 unique variants with a total of 103,428 reads or copies. Note: the wild-type API P2-P1 sequence is PM.

P2-P1 Residues	Abundance
DA	23191
SS	11369
PM	10126
PL	6718
DA	6572
PL	5882
GT	3490
DV	2863
GA	1782
PS	1508
DT	1455
DS	1241
PS	1005
DV	1002
PM	921
PA	860
PS	819
PS	751
DS	747
PT	744

Table 4: Top 20 Most Abundant Variants in the 5th Round NEG Biopan.

The repeating variants were a result of different nucleic acid sequences expressing the same peptide. The numbers shown in this table represent the reads or copies of variants from the deep sequencing data. There was a total of 525 unique variants with a total of 90,956 reads or copies. "-" indicates a stop codon. Note: the wild-type API P2-P1 sequence is PM.

P2-P1 Residues	Abundance
GG	38309
-L	14444
PA	5035
PP	4808
PD	3959
SQ	3461
GN	2403
FS	2356
PP	1398
PT	1352
EP	1351
PA	1330
VG	1254
QP	1220
DI	1184
TD	1073
IY	977
PP	951
LS	757
LS	751

5.3 Biopanning the API-P4P1' Phage Library with PR3

The deep sequencing parameters explained in the Methods (see Section 4.2) resulted in 7,495 unique nucleic acid variants in the unselected/original library. All rounds of biopanning for the API-P4P1' were deep sequenced. The 5th round biopanning results showed the presence of 605 different API variants in the EXP condition and 617 in the NEG condition. The top 20 most abundant nucleotide sequences were translated and analysed. The enrichment of those variants in the EXP condition was quantified and shown in Table 5 and Figure 5. The most abundant P4-P1' sequence in the EXP library was A355-I356-D357-A358-S359 (designated API-DA since the residues at the other three positions were wild-type) at 69,513 copies. This dipeptide was the same amino acid sequence that was the most abundant in the biopanning of the API-P2P1 library. The second most enriched sequence was A355-I356-P357-M358-N359 (API-N) at 35,030 copies. API-N was the 8th and API-DA was the 12th most abundant variant in the 5th round of the NEG control. However, this was their abundance at the particular screen only. Based on their enrichment level (or lack thereof) within the NEG control screens and their significant enrichment in the EXP condition, they were considered viable options for kinetic characterization with PR3 (Table 6 and Figure 6). A consensus motif of AI - - S was also observed in 27 (54%) variants in the top 50 selected variants in Round 5 of screening (Table 7).

Table 5: Abundance of the Top 20 Variants in the API-P4P1' Library.

"R-0" indicates the initial, unselected library. There are two "AITTS" sequences represented in this table. Each of those variants was expressed by different nucleic acid sequences, resulting in the observed repetition. Note: the wild-type sequence at the P4-P1' is AIPMS.

	AIDAS	AIPMN	AISSS	AISTS	AINTS
R-0	32	36	33	85	32
R-1	940	881	529	614	535
R-2	7766	6182	2779	1476	1439
R-3	23298	18226	5516	2551	2298
R-4	34093	28608	4196	1966	1792
R-5	69513	35030	3759	2002	1747
	AINAS	**AIDLS**	**AISVS**	**RSYGC**	**ALTSS**
R-0	162	26	36	28	20
R-1	1489	213	374	1642	357
R-2	2908	543	1522	691	648
R-3	2934	820	1937	267	593
R-4	1301	660	1100	1388	563
R-5	854	703	687	624	536
	AITTS	**SLTSG**	**MLDTT**	**TISST**	**AIPTS**
R-0	48	16	18	55	55
R-1	370	58	238	308	667
R-2	889	260	631	627	924
R-3	947	339	681	722	876
R-4	593	722	393	556	490
R-5	427	403	377	360	326
	AITTS	**ANSVS**	**SHHIT**	**AIELS**	**AIGAS**
R-0	42	74	39	27	23
R-1	353	853	393	235	259
R-2	848	1042	963	379	637
R-3	818	471	592	391	348
R-4	387	235	272	222	188
R-5	315	184	151	135	127

Figure 5: Enrichment Graph of the Top 20 Variants from the API-P4P1' Library. The abundance of the variants (at right) is shown, in number of deep sequencing reads, versus the round number of biopanning. This graph demonstrates the abundance of the top 20 variants from the 5th round of biopanning, throughout the entire screening protocol. Only AIDAS (API-DA) and AIPMN (API-N) were enriched through the different screening experiments. Note: the wild-type sequence at P4-P1' is AIPMS.

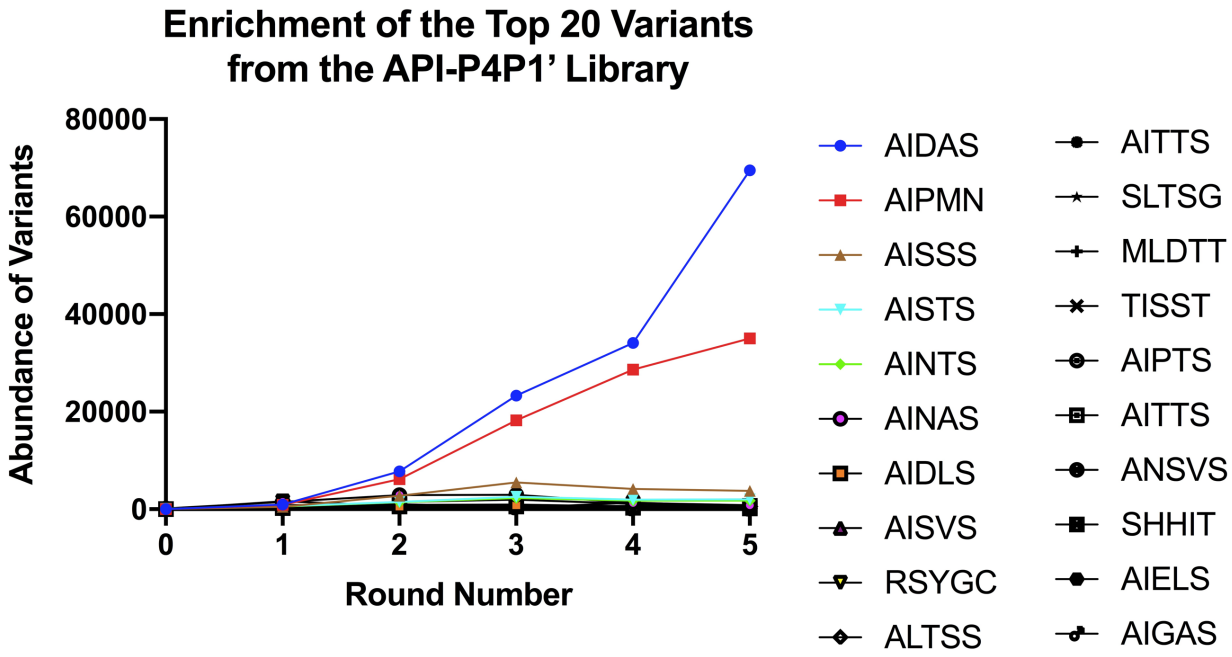
Enrichment of the Top 20 Variants
from the API-P4P1' Library
Abundance of Variants
80000
60000
40000
20000
0
0
1
2
3
4
5
Round Number
AIDAS
AIPMN
AISSS
AISTS
AINTS
AINAS
AIDLS
AISVS
RSYGC
ALTSS
AITTS
SLTSG
MLDTT
TISST
AIPTS
AITTS
ANSVS
SHHIT
AIELS
AIGAS

Table 6: Abundance of the Top 20 Variants in the NEG Control API-P4P1' Library.

"R-0" indicates the initial, unselected library.

	RSYGC	TPLKP	HIRTF	VTKAY	GVPAY
R-0	28	48	32	53	46
R-1	21	128	56	117	98
R-2	6136	6572	3291	986	690
R-3	8851	2661	3030	664	182
R-4	19738	17951	6520	7481	1792
R-5	44065	29997	11832	3520	2777
	RSDHS	**AIPMN**	**TIRDE**	**RKLS-**	**PPNLQ**
R-0	20	36	24	56	47
R-1	87	11	182	0	94
R-2	1961	199	6471	336	2040
R-3	746	1041	3634	189	1323
R-4	716	108	2340	539	1368
R-5	2035	1965	1607	1549	1374
	RDLIQ	**AIDAS**	**AIPTS**	**STSIP**	**LCH-V**
R-0	20	32	44	12	40
R-1	106	2	62	89	54
R-2	0	2	49	297	118
R-3	504	1444	33	239	34
R-4	2569	1092	0	931	339
R-5	1281	1183	1090	871	516
	QIMYQ	**YHYAR**	**TISST**	**TRARH**	**KSVKD**
R-0	50	29	55	41	10
R-1	149	32	8	211	128
R-2	943	0	924	850	0
R-3	563	28	774	500	87
R-4	3058	164	937	494	835
R-5	456	436	391	92	68

Figure 6: Enrichment Graph of the Top 20 Variants from the NEG Control Screens of the API-P4P1' Library.

The abundance of the variants (at right) is shown, in number of deep sequencing reads, versus the round number of biopanning. This graph demonstrates the enrichment of the top 20 variants in the NEG condition from the 5th round of biopanning throughout the entire screening protocol. Even though API-DA and API-N both appeared in the top 20 most abundant variants in the 5th round of screening, they were not substantially enriched over the 5 rounds of screening without the selective pressure of PR3.

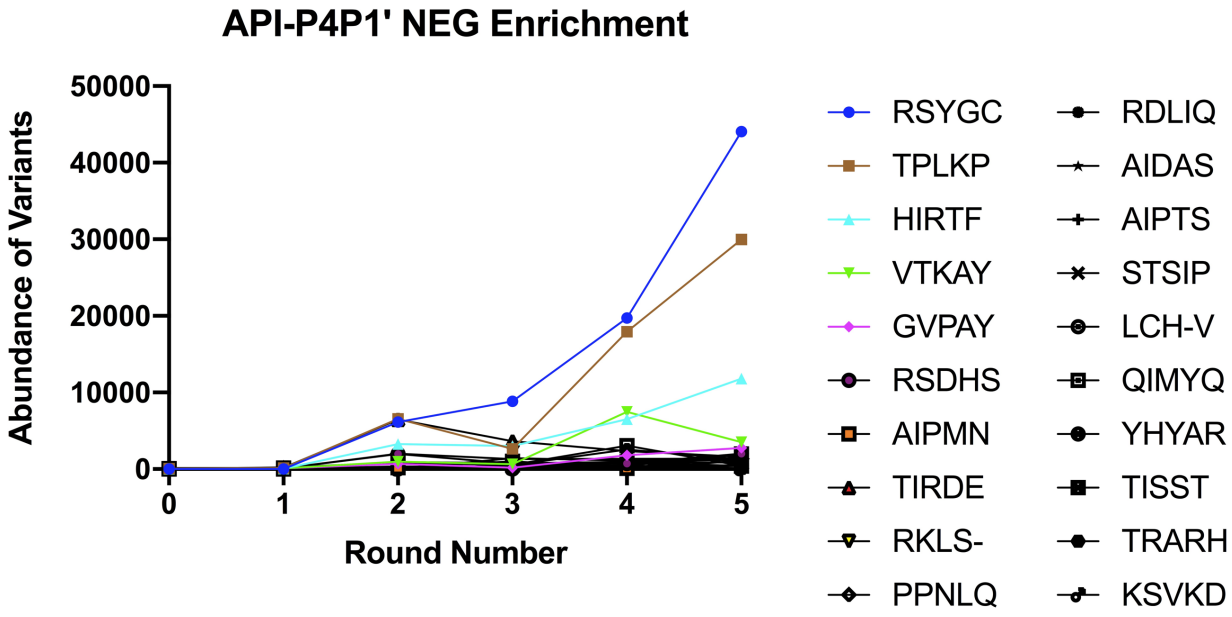
API-P4P1' NEG Enrichment
Abundance of Variants
50000
40000
30000
20000
10000
0
0
1
2
3
4
5
Round Number
RSYGC
TPLKP
HIRTF
VTKAY
GVPAY
RSDHS
AIPMN
TIRDE
RKLS-
PPNLQ
RDLIQ
AIDAS
AIPTS
STSIP
LCH-V
QIMYQ
YHYAR
TISST
TRARH
KSVKD

Table 7: Consensus Motif in the Top 50 Most Abundant Variants in Round 5 API-P4P1' Library.

The sequence motif AI - - S where the P4, P3 and P1' residues are conserved to alanine, isoleucine and serine respectively appears in 27 variants out of the top 50 selected variants after 5 rounds of screening.

AIDAS	NQATQ
AIPMN	TIRDE
AISSS	AMPIT
AISTS	AYNAS
AINTS	AIDAS
AINAS	TPLKP
AIDLS	AIDAS
AISVS	AIDAS
RSYGC	AIDAS
ALTSS	AIPMN
AITTS	QITAN
SLTSG	AIDAS
MLDTT	SRNTV
TISST	AIPVS
AIPTS	AIDAS
AITTS	AITMS
ANSVS	AISLS
SHHIT	GVPAY
AIELS	AIDAS
AIGAS	PPTKN
AIGAS	AIDAS
TVATT	AIDAS
AIETS	GIDLA
AIPTS	HIRTF
FMDSA	RRVHD

5.4 Screening the Round 3 PR3-selected Candidates in Bacterial Lysates

As was done in a previously published API biopanning study from our laboratory[60], the entire API-encoding DNA population was mobilized after three rounds of PR3 biopanning and transferred into a pBAD plasmid background. This is a plasmid directing soluble cytoplasmic expression of unfused API variants. Round 3 was selected over Round 5 (as in the analogous published approach) because of the abundance of API-DA in Round 5 phage and our desire to probe the functionality of other candidates as PR3 inhibitors (see Figure 5).

Prior to applying this technique to the current project, it was necessary to determine if PR3 could be substituted for thrombin in the previously published study, as the proteinase bound to microtiter plate wells, and remain competent for API binding in that setting. Two optimization reactions were therefore done. The results from the first test (Figure 7) indicated that immobilized PR3 bound more avidly to purified API proteins than to API contained in lysates. API-WT was expected to bind PR3 avidly and API-R was expected to bind PR3 less effectively.[50,67] The optical density signal for immobilized purified API-WT (1.0 ± 0.4, mean ± SD, n=4) was greater than that for purified API-R (0.20 ± 0.006, n=4) and both were higher than blank wells (0.010 ± 0.006, n=2); the difference between API-WT and API-R lysates was less substantial (0.051 ± 0.021 versus 0.027 ± 0.05, n=2). This test also included fXIa-coated wells as a positive control for this assay. Only API-R resulted in a substantial signal (1.28 ±0.097, n=1), as expected from previous studies (Figure 8).[60]

The results shown in Figure 7 were obtained with lysates from 1mL of bacterial culture. This amount was raised to 2mL in the experiment shown in Figure 9. This change in procedure produced a more substantial difference between API-WT lysates (0.15 ± 0.01) and API-R lysates (0.08 ± 0.02) than the previous approach and was adopted for screening of unknown candidate lysates.

Of the 32 screened colonies, 8 produced a positive signal indicating possible high binding of an API variant to PR3. All 8 were selected for Sanger sequencing. Three of the plasmids showed indeterminate results, whereas the remaining 5 produced the same sequence at the P4-P1' RCL positions: GCT ATT CCG ATG AAT (AIPMN residues). This was the second most enriched variant in the API-P4P1' phage library (Table 5 and Figure 5). It differs from WT at only position (P1', S359N). This variant was therefore designated API-N. The data from the screens is shown in Figure 10.

Figure 7: Results of First Mass Lysate Optimization Test with PR3-Coated Wells. Lysates were made from bacteria contained in 1mL of cell culture. The lysates were added onto microtiter wells coated with 1µg/mL PR3. In addition to bacterial lysates, 2.5-5µg/mL of purified API-DA and API-WT were also added. The Y-axis shows the mean optical densities at 450nm for all the samples. The mean of duplicate (n=2) determinations ± SEM is shown for each sample.

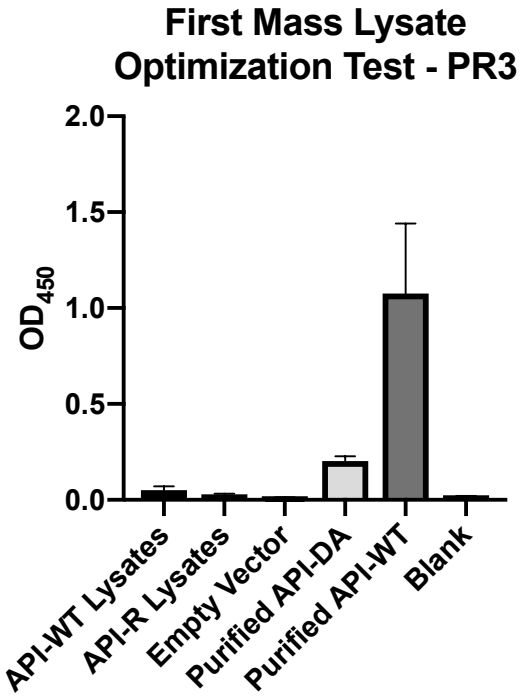
First Mass Lysate
Optimization Test - PR3
OD450
2.0
1.5
1.0
0.5
0.0
API-WT Lysates
API-R Lysates
Empty Vector
Purified API-DA
Purified API-WT
Blank

Figure 8: Results of First Mass Lysate Optimization Test with fXIa-Coated Wells. Lysates were made from bacteria contained in 1mL of cell culture. The lysates were added onto microtiter wells coated with 0.1µg/mL fXIa. In addition to bacterial lysates, 5µg/mL of purified API-DA and API-WT were also added. The Y-axis shows the mean optical densities at 450nm for all the samples. The mean of duplicate (n=2) determinations ± SEM is shown for each sample.

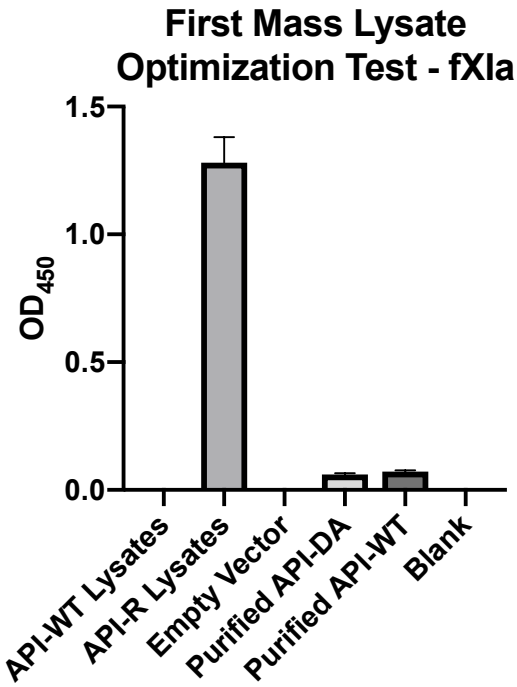
First Mass Lysate
Optimization Test - fXIa
1.5
1.0
0.5
0.0
OD450
API-WT Lysates
API-R Lysates
Empty Vector
Purified API-DA
Purified API-WT
Blank

Figure 9: Results of the Second Mass Lysate Optimization Test with PR3-Coated Wells.

Lysates were made from bacteria contained in 2mL of cell culture. The lysates were added onto microtiter wells coated with 1µg/mL PR3. The Y-axis shows the mean optical densities at 450nm for all the samples. The mean of duplicate (n=2) determinations ± SEM is shown for each sample.

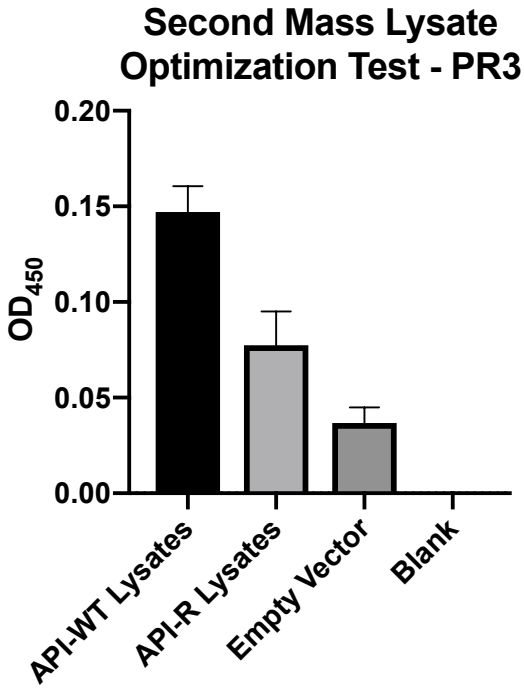
Second Mass Lysate
Optimization Test - PR3
0.20
0.15
0.10
0.05
0.00
OD450
API-WT Lysates
API-R Lysates
Empty Vector
Blank

Figure 10: Mass Lysate Screening Results.

The mean optical density at 450nm for each sample is shown on the Y-axis. The red bars indicate PR3-lysate binding "hits" that were then further analyzed because their optical densities were above the range of values for API-R. The yellow bar indicates API-WT lysates, green bar indicates API-R lysates, and blue bar indicate empty vector-transformed cell lysates. All wells in this screen were coated with 1μg/mL PR3. The mean of duplicate (n=2) determinations ± SEM is shown for each colony and control.

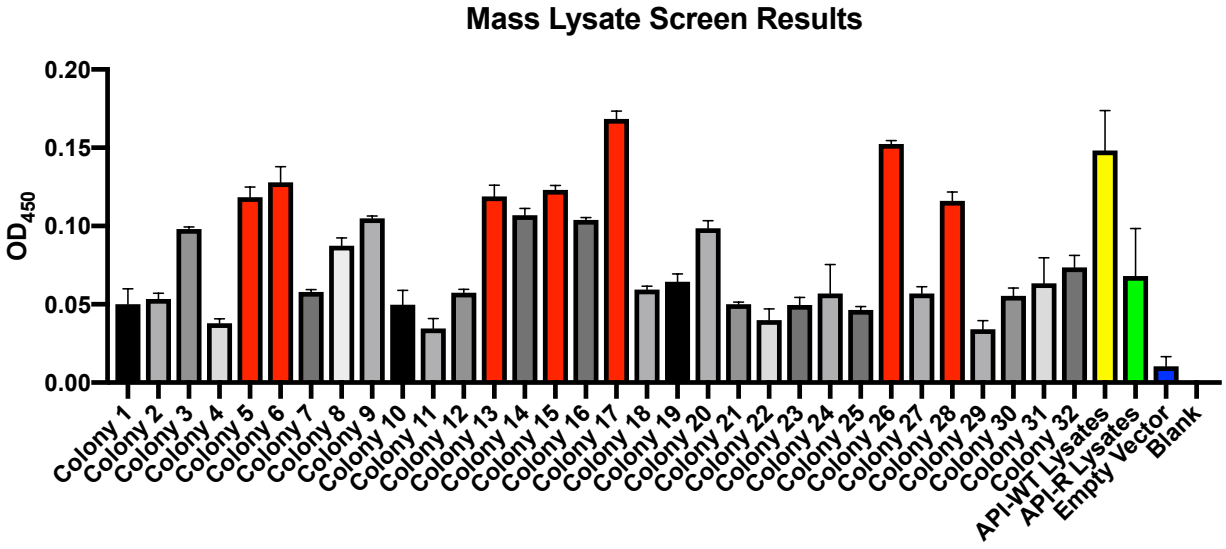
Mass Lysate Screen Results
OD450
0.20
0.15
0.10
0.05
0.00
Colony 1
Colony 2
Colony 3
Colony 4
Colony 5
Colony 6
Colony 7
Colony 8
Colony 9
Colony 10
Colony 11
Colony 12
Colony 13
Colony 14
Colony 15
Colony 16
Colony 17
Colony 18
Colony 19
Colony 20
Colony 21
Colony 22
Colony 23
Colony 24
Colony 25
Colony 26
Colony 27
Colony 28
Colony 29
Colony 30
Colony 31
Colony 32
API-WT Lysates
API-R Lysates
Empty Vector
Blank

5.5 Recombinant Histidine-Tagged and Glutathione-S-Transferase Fusion Protein Purification

To assess the reactivity of the variant API proteins identified in the phage display and bacterial lysate screening experiments, it was necessary to express and purify them. An expression system similar to that previously published by our laboratory was employed[46,68,69], in that API proteins were expressed as soluble proteins in the *E. coli* cytoplasm. They were expressed as GST fusion proteins to enhance yield and separated from the GST domain by cleavage at a human rhinovirus type 14 3C proteinase site (HRV3C Proteinase, Thermo Scientific). The API moiety contained an N-terminal hexahistidine tag for further purification after proteolytic elution from a glutathione-sepharose resin. A schematic diagram of the pGEX-API plasmid containing those domains is shown in Figure 11.

Elution fractions from the glutathione-sepharose and Ni-NTA columns from the purification of API-WT, API-DA and API-N were electrophoresed on 10% SDS-PAGE gels as shown in Figures 12, 13, and 14, respectively. *E. coli* BL21 cell cultures transformed with pGEX-API-(WT or DA or N) and induced with IPTG expressed an abundant polypeptide of 74 kDa. Most of this protein remained insoluble and was not mobilized into the cleared lysate following sonication and clarification. Elution of protein bound to the glutathione-sepharose column with HRV3C Proteinase released a 48 kDa protein with the expected mobility of hexahistidine-tagged API. Subsequent elution of the glutathione-sepharose column with glutathione released a small quantity of uncleaved 74 kDa fusion protein, a larger quantity of 26 kDa protein (the expected mobility of GST)

and a small quantity of 48 kDa protein. The latter was either API protein that remained associated with the column despite its liberation from GST residues, or GST-tagged HRV3C Proteinase (termed “Precision Protease” by its manufacturers), which coincidentally had the same mobility. The mobility of the presumptive API band (48 kDa) and presumptive GST band (26 kDa) was consistent with their being cleavage products of the presumptive GST-API band (74 kDa). The presumptive API polypeptide eluting from the Ni-NTA column was the only stained band in the preparation, and its identity was subsequently confirmed by immunoblotting and inhibitory activity. Expression and purification of all three API variants (WT, DA and N) resulted in similar concentrations of purified protein at approximately 1mg/mL.

Figure 11: Schematic Diagram of the pGEX-API Plasmid.

In this figure, the GST-API open reading frame (ORF) is highlighted, with the GST protein being expressed at the N-terminus of the GST-API protein, followed by the hexahistidine-tag (specific sequence not shown) then the API protein. The AmpR gene ORF is also shown that codes for the antibiotic resistance protein within the bacteria, allowing the growth of *E. coli* on ampicillin-rich LB+agar plates. The lacl repressor gene, which inhibits the expression of lactases within the bacteria is also shown, with the origin of replication (ori) embedded between it and the AmpR gene segment. Finally, written on the outer border of the schematic are the restriction sites within the plasmid that cleave a single time.

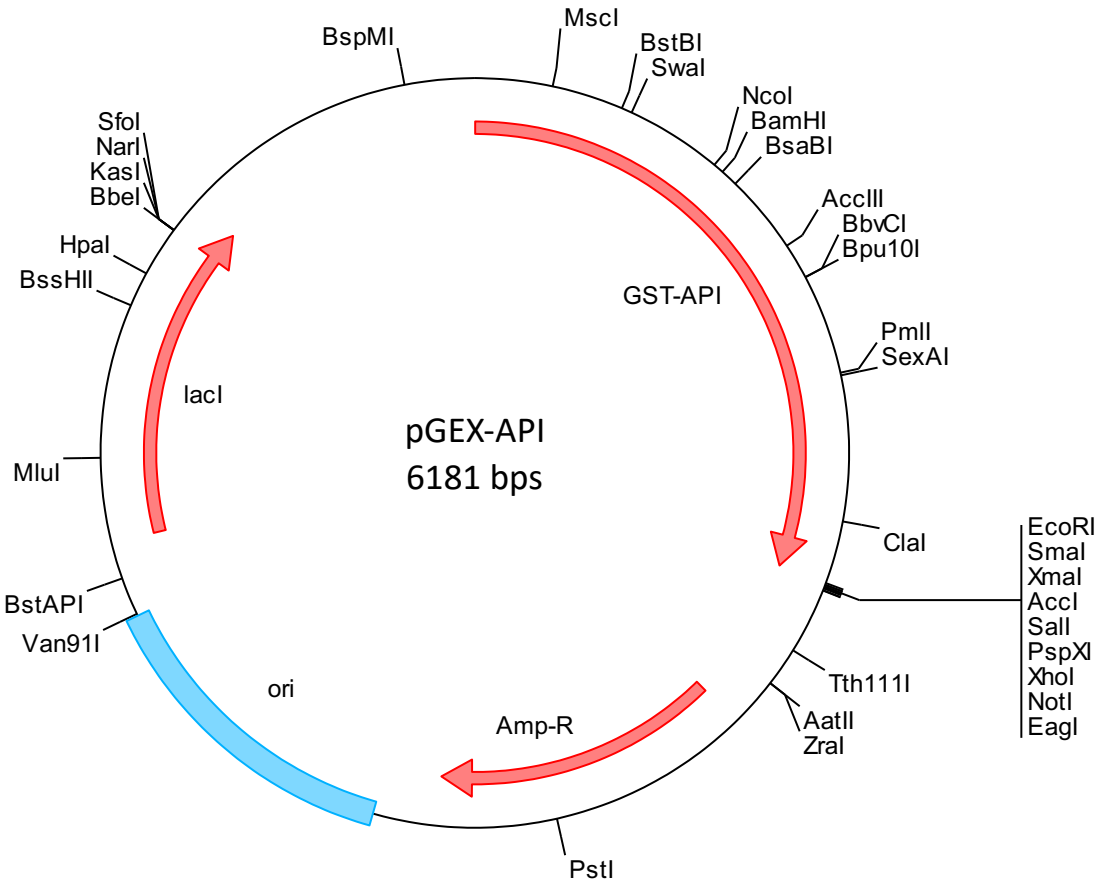
pGEX-API
6181 bps
GST-API
lacI
ori
Amp-R
BspMI
MscI
BstBI
SwaI
NcoI
BamHI
BsaBI
AccIII
BbvCI
Bpu10I
PmlI
SexAI
ClaI
EcoRI
SmaI
XmaI
AccI
SalI
PspXI
XhoI
NotI
EagI
Tth111I
AatII
ZraI
PstI
Van91I
BstAPI
MluI
BssHII
HpaI
BbeI
KasI
NarI
SfoI

Figure 12: Purification of API-WT Expressed in *E. coli* BL21 Cells.

A Coomassie Brilliant Blue-stained 10% SDS-acrylamide gel is shown. The samples were not loaded onto the gels in the temporal order of the purification scheme. Each sample was electrophoresed under reducing conditions. Aliquots of fractions generated during purification, identified above the lanes, are shown. The Cleared Lysate was loaded onto a glutathione-sepharose column, generating a Flow-Through (FT Lysate). Following washing (Wash, fifth lane from left), the glutathione-sepharose column was eluted by on-column cleavage with HRV3C Proteinase to generate the Ni-NTA Input (tenth lane from left), flow-through (FT) and wash (Wash). The glutathione-sepharose column was eluted with 2mM glutathione and elution fractions 1, 3, and 5 were electrophoresed. The Ni-NTA column was eluted with Imidazole buffer as indicated in Methods; fractions 1,3,5, and 7 are shown. Marker lanes contain PageRuler Protein Ladder (Thermo Scientific); the position of the 70, 50, and 30 kDa markers is identified on both lanes.

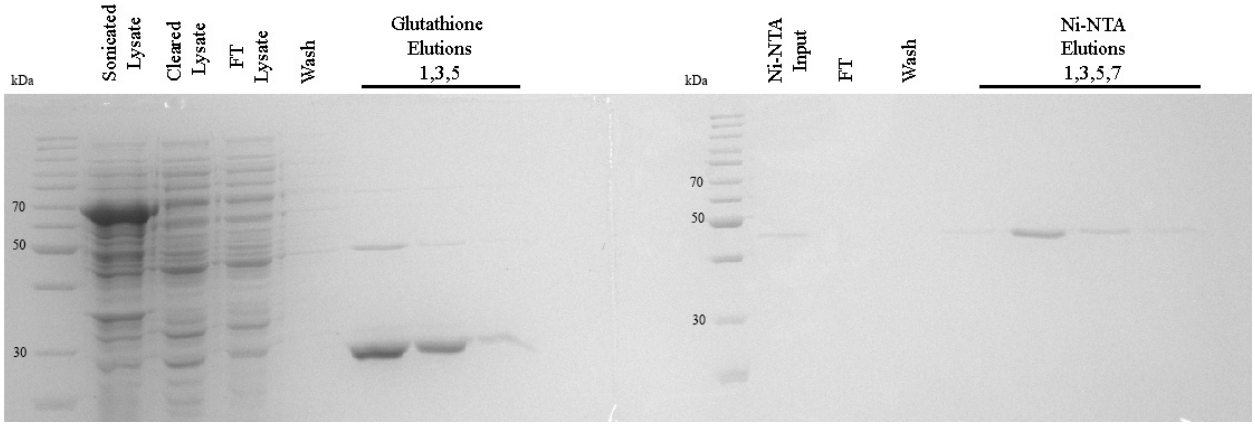
kDa
Sonicated Lysate
Cleared Lysate
FT Lysate
Wash
Glutathione Elutions 1,3,5
70
50
30
kDa
Ni-NTA Input
FT
Wash
Ni-NTA Elutions 1,3,5,7
70
50
30

Figure 13: Purification of API-DA Expressed in *E. coli* BL21 Cells.

A stained gel identical to that in Figure 12 is shown, except that API-DA rather than API-WT was purified, and elution fractions 1-4 are shown both for the glutathione-sepharose column with glutathione (underlined lanes, at left) and the Ni-NTA agarose column (underlined lanes, at right).

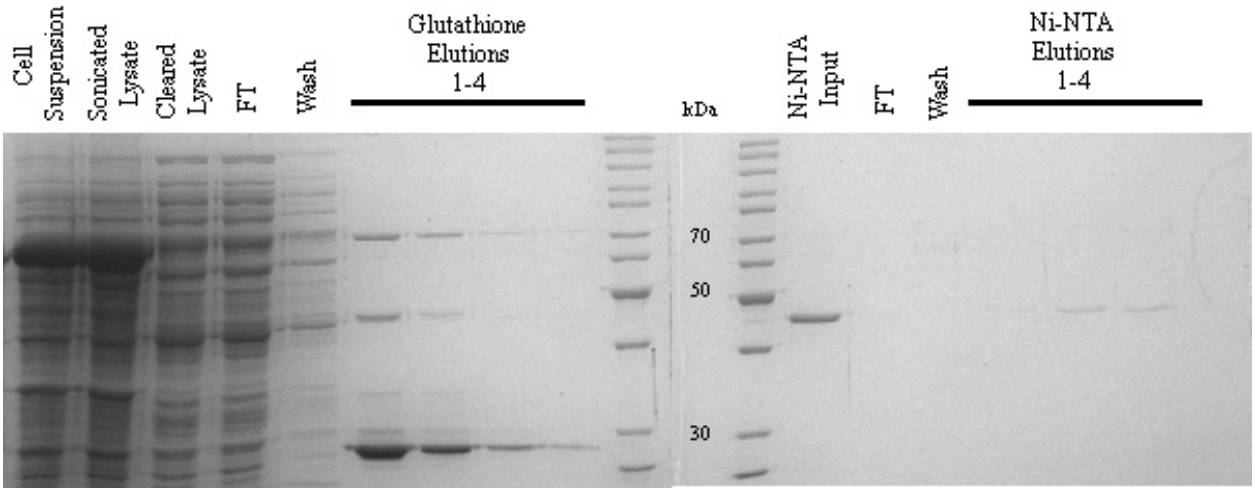
Cell Suspension
Sonicated Lysate
Cleared Lysate
FT
Wash
Glutathione Elutions 1-4
kDa
70
50
30
Ni-NTA Input
FT
Wash
Ni-NTA Elutions 1-4

Figure 14: Purification of API-N Expressed in *E. coli* BL21 Cells.

A stained gel identical to that in Figure 12 is shown, except that API-N rather than API-WT was purified.

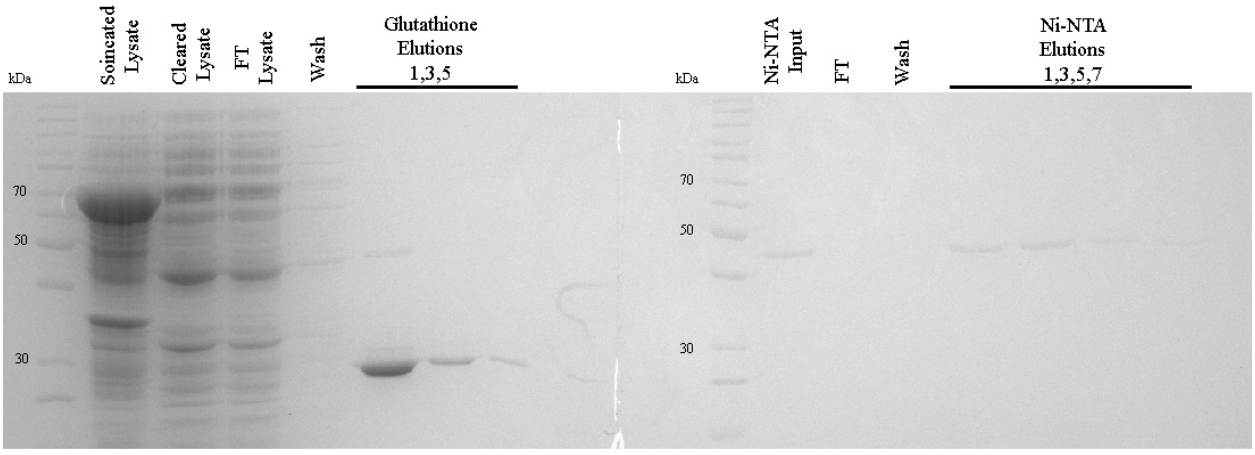
kDa
Soincated Lysate
Cleared Lysate
FT Lysate
Wash
Glutathione Elutions 1,3,5
70
50
30
kDa
Ni-NTA Input
FT
Wash
Ni-NTA Elutions 1,3,5,7
70
50
30

5.6 Serpin-Proteinase 3 Gel-Based Complexing Assay

Purified recombinant API proteins were reacted with purified PR3 for 5 minutes, at different molar ratios, and the reaction products were analyzed by SDS-PAGE (Figures 15, API-WT and Figure 16, API-N). In both cases, at high serpin: proteinase ratios, reaction samples revealed a novel polypeptide not found in either recombinant API preparation or in that of PR3, of a mobility consistent with a size of 72 kDa. This polypeptide species was consistent with the anticipated size of covalently bonded PR3 and API 1-358 (with API 359-394 C-terminal fragment separating on reducing SDS-PAGE). Proteolytic digestion products migrating with a more rapid mobility than recombinant API were also observed; the major species in both API-WT and API-N reactions with PR3 was of approximately 44 kDa, consistent with its being API 1-358. Such a reaction product is consistent with API-WT and API-N serving in part as a substrate for PR3 cleavage and in part as an inhibitor.

The gel-based complexing assays for API-N and API-WT showed the presence of presumptive API-PR3 complex bands of 72 kDa at all API to PR3 ratios (Figures 15 and 16). The 10:1 and 5:1 API to PR3 reactions showed the presence of more intense presumptive complex bands compared to the 1.5:1 ratio reactions. However, the complex bands were very faint on a stained SDS-PAGE gel, suggesting that an immunoblot could serve as a more sensitive method to visualize the bands.

In contrast to the complexing assay results for API-WT and API-N, reaction of recombinant API-DA yielded little or no stainable API-PR3 complexes; instead, the predominant reaction product at all ratios tested was cleaved API-DA, with a mobility

corresponding to the ~4 kDa reduction anticipated for separation of API-DA 359-394 from the rest of the protein (Figure 17).

Figure 15: Reaction of API-WT and PR3 at Different Molar Ratios.

A Coomassie Brilliant Blue-stained 10% SDS-PAGE gel is shown, with molecular mass markers at left. The red boxes highlight the presence of the presumptive API-WT-PR3 complex band at around 72 kDa.

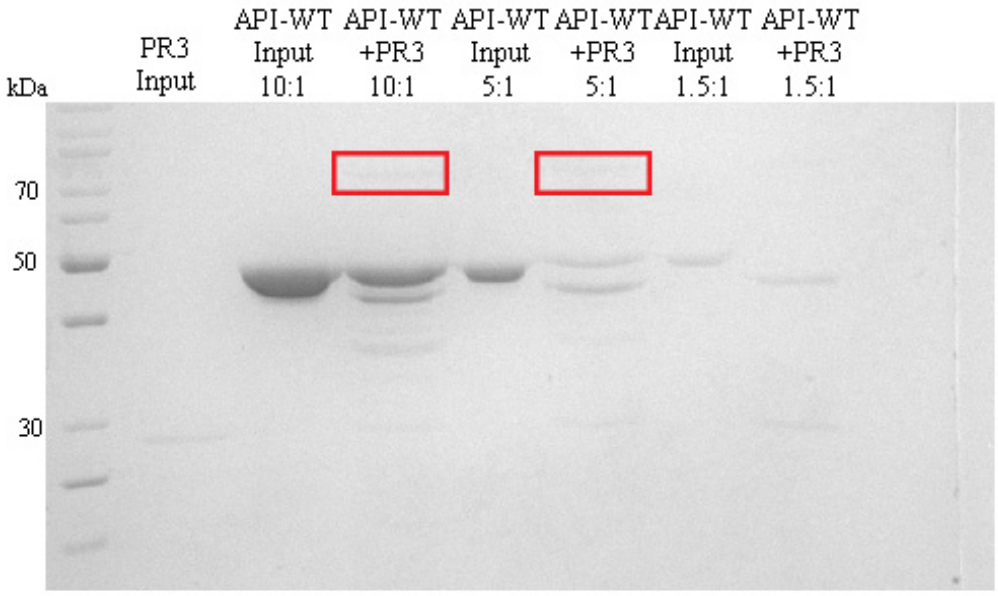
kDa
PR3 Input
API-WT Input 10:1
API-WT +PR3 10:1
API-WT Input 5:1
API-WT +PR3 5:1
API-WT Input 1.5:1
API-WT +PR3 1.5:1
70
50
30

Figure 16: Reaction of API-N and PR3 at Different Molar Ratios.

A Coomassie Brilliant Blue-stained 10% SDS-PAGE gel is shown, with molecular mass markers at left. The red boxes highlight the presence of the presumptive API-N-PR3 complex band at around 72 kDa.

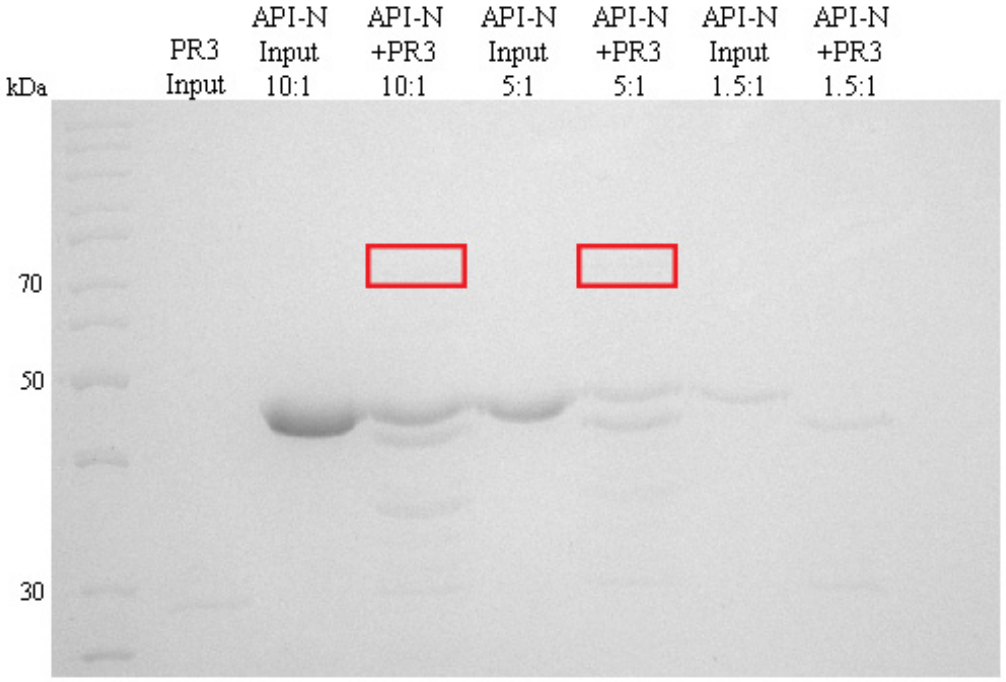
kDa
PR3 Input
API-N Input 10:1
API-N +PR3 10:1
API-N Input 5:1
API-N +PR3 5:1
API-N Input 1.5:1
API-N +PR3 1.5:1
70
50
30

Figure 17: Reaction of API-DA and PR3 at Different Molar Ratios.

A Coomassie Brilliant Blue-stained 10% SDS-PAGE gel is shown, with molecular mass markers at left.

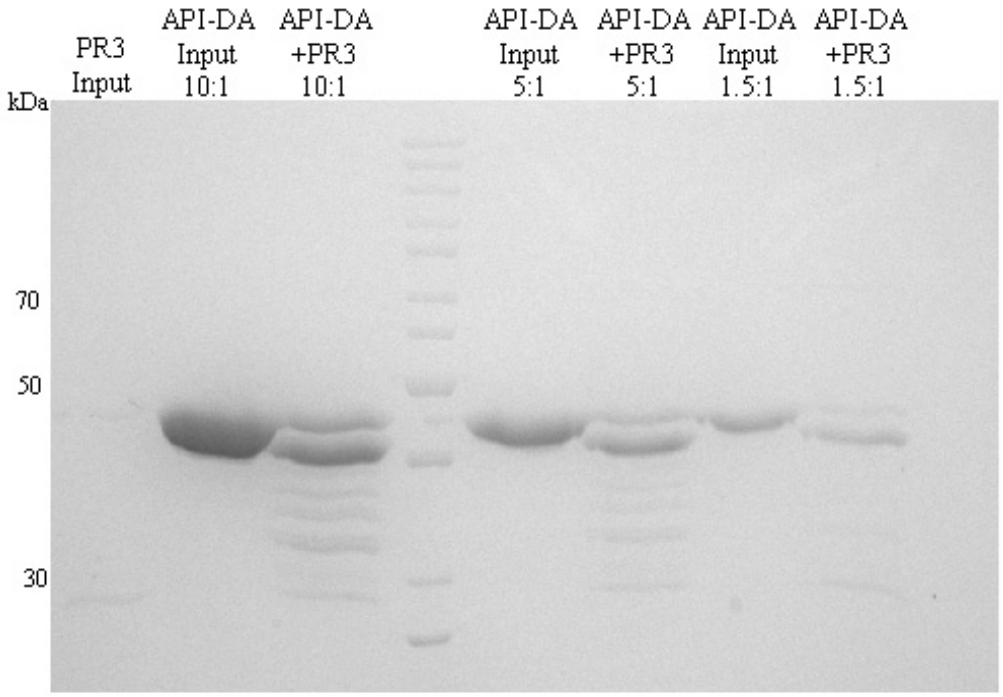
PR3 Input
API-DA Input 10:1
API-DA +PR3 10:1
API-DA Input 5:1
API-DA +PR3 5:1
API-DA Input 1.5:1
API-DA +PR3 1.5:1
kDa
70
50
30

5.7 Unsuccessful k_2 determination using FRET Substrate

Using a FRET substrate was not successful in measuring the k_2 for the API-PR3 interaction. With multiple trials of the method described in Section 4.14, none produced a linear curve to calculate the k_2 of the reaction. Figure 18 shows the most "linear" curve produced from the API-WT+PR3 reaction at a 1:1 ratio. However, we could not reproduce or improve this trial, as seen in trials 2 and 3 (Figure 19). These results made us change our approach and rely on gel-based kinetic assays.

Figure 18: k_2 Determination of the API-WT-PR3 Interaction using a FRET Substrate (Trial 1).

The FRET substrate used in this experiment was Abz-Val-Ala-Asp-Nva-Arg-Asp-Arg-Gln-EDDnp (Peptides International).

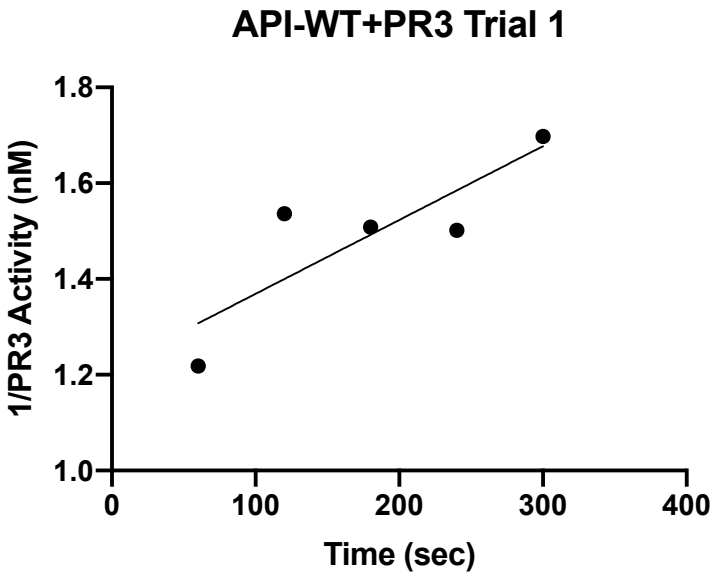

$Y = 0.001542*X + 1.215$

$R^2 = 0.7146$

Figure 19: k_2 Determination of the API-WT-PR3 Interaction using a FRET Substrate (Trials 2 and 3).

The FRET substrate used in these experiments was Abz-Val-Ala-Asp-Nva-Arg-Asp-Arg-Gln-EDDnp (Peptides International).

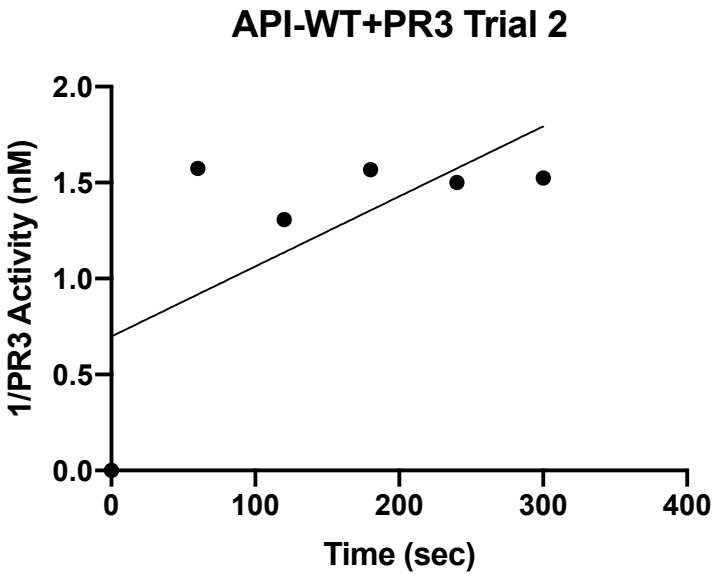

$Y = 0.003649*X + 0.6986$

$R^2 = 0.4390$

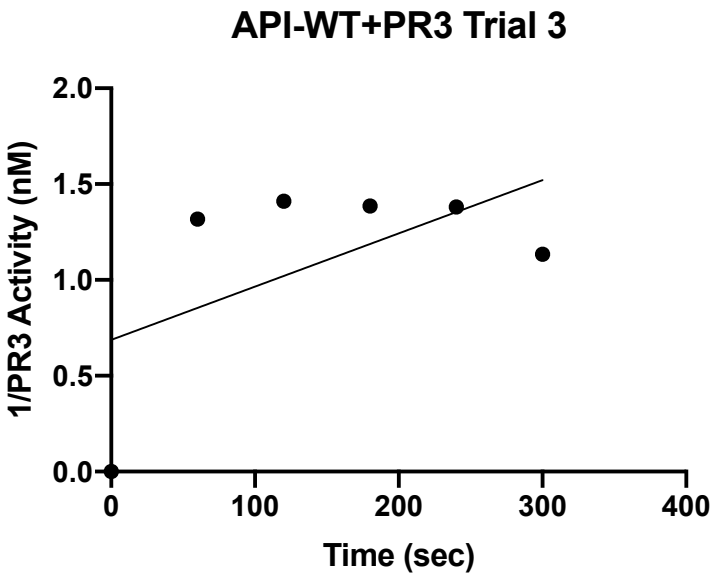

$Y = 0.002778*X + 0.6879$

$R^2 = 0.3210$

5.8 Determination of the Second Order Rate Constant for API-WT Inhibition of PR3

Anti-API immunoblots were used to follow the formation of API-WT-PR3 complexes over time, in order to determine the k_2 for the reaction (as shown in Figure 20). Note that the immunoreactivity of the 72 kDa presumptive API-WT-PR3 complex with specific anti-API antibodies, and its absence from either purified API-WT or PR3 preparations, confirmed its identity. The blots demonstrated an increase in complex formation over time. The band intensities were plotted against time (Figure 21) and the average k_2^* value of all 5 trials was calculated using a previously established method in our lab.[60] The API-WT+PR3 experiments yielded a k_2^* of 1.16×10^5 arbitrary intensity units^{-1}s^{-1} $\pm 0.53 \times 10^5$ ($\pm$45%). As indicated by the units, this k_2^*, although proportional to the real k_2, is not the true value, as it is based on arbitrary intensity units rather than molar concentrations of API. To obtain the true k_2 value, the change in complex band intensity was calibrated with known molar concentrations of API (see Sections 4.16 and 5.10).

Figure 20: Immunoblots of API-WT+PR3 Gel-Based Kinetic Experiment.

Trials 1-5, with trial 1 shown in the upper left panel, trial 2 in the upper right panel, trial 3 in the middle left panel, trial 4 in the middle right panel, and trial 5 in the lower left panel.

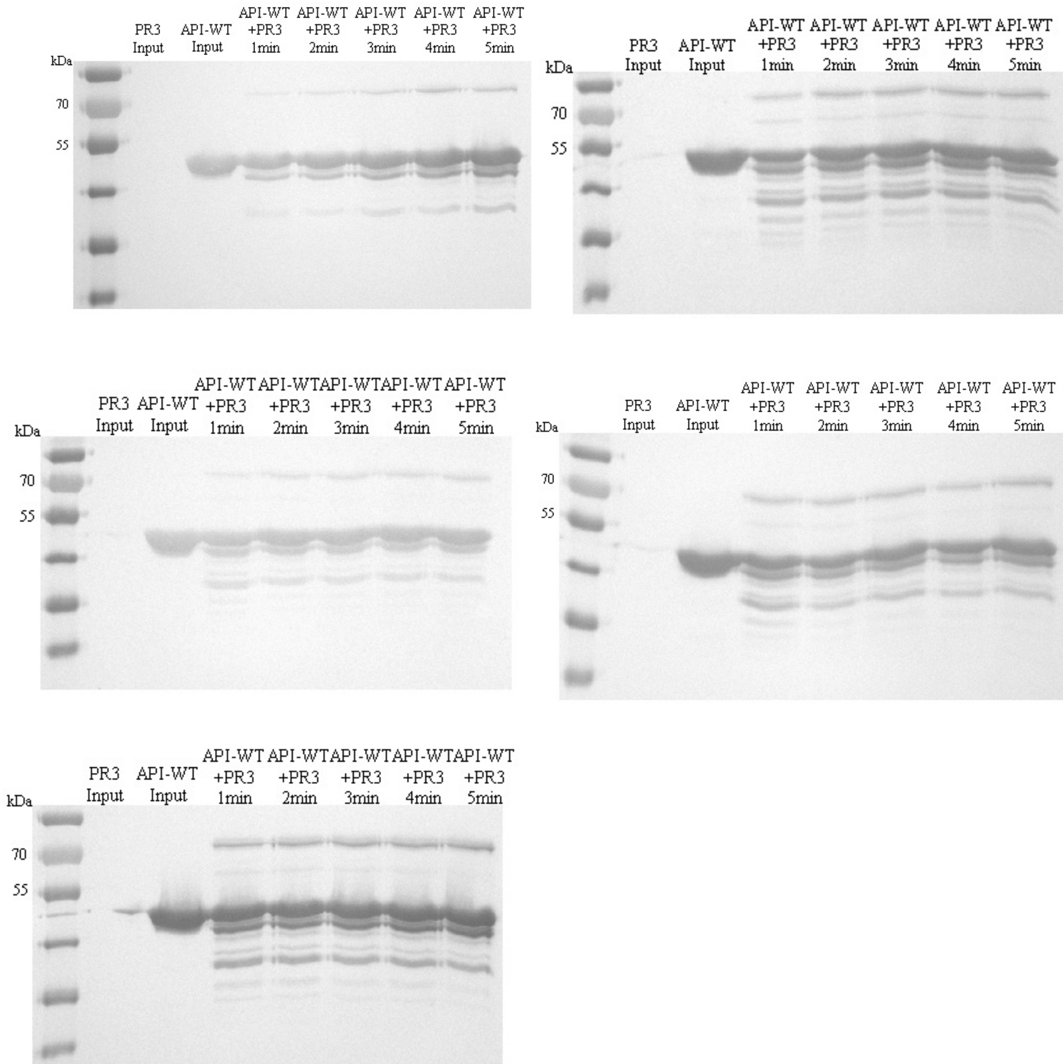
kDa
70
55
PR3 Input
API-WT Input
API-WT +PR3 1min
API-WT +PR3 2min
API-WT +PR3 3min
API-WT +PR3 4min
API-WT +PR3 5min

Figure 21: API-WT+PR3 Kinetic Analysis Plots.

Gel-based kinetic analysis of API-WT and PR3 binding showing the progression of inhibitory complex formation between the two proteins over 5 minutes (trials 1-5). These graphs correspond to the immunoblots shown in Figure 18.

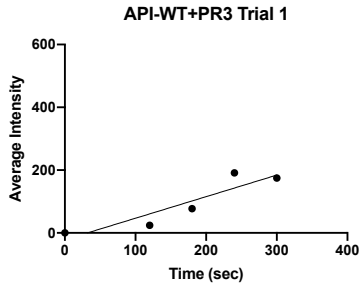

Y = 0.6869*X - 21.88

R^2 = 0.8390

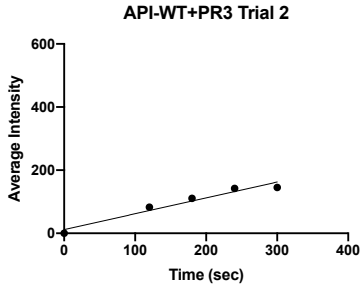

Y = 0.5025*X + 11.78

R^2 = 0.9496

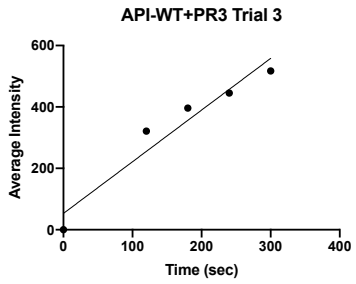

Y = 1.683*X + 53.16

R^2 = 0.9317

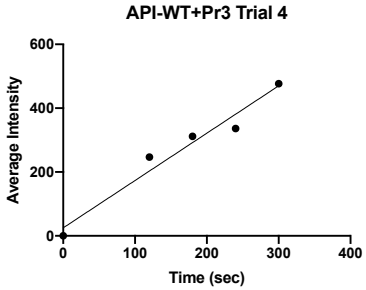

Y = 1.483*X + 25.10

R^2 = 0.9002

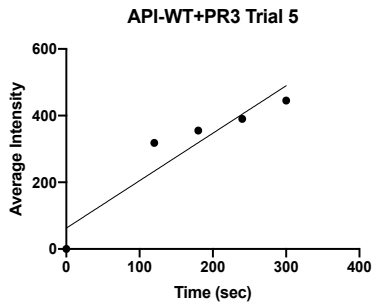

Y = 1.424*X + 62.60

R^2 = 0.8809

5.9 Determination of the Second Order Rate Constant for API-N Inhibition of PR3

The immunoblots of the API-N reactions with PR3 are shown in Figure 22. The blots demonstrated an increase in complex formation over time, similar to API-WT. The band intensities were plotted against time (Figure 23) and the average k_2^* value of all 5 trials was calculated, as mentioned earlier.[60] The API-N+PR3 experiments yielded a k_2^* of 1.10×10^5 arbitrary intensity units^{-1}s^{-1} $\pm 0.34 \times 10^5$ ($\pm$31%), which was not significantly different than API-WT (Table 8). The data was analyzed using an unpaired t-test and yielded a p-value of 0.8244 (see Sections 4.16 and 5.10 for complex band calibration).

Figure 22: Immunoblot of API-N+PR3 Gel-Based Kinetic Experiment.

Trials 1-5, with trial 1 shown in the upper left panel, trial 2 in the upper right panel, trial 3 in the middle left panel, trial 4 in the middle right panel, and trial 5 in the lower left panel.

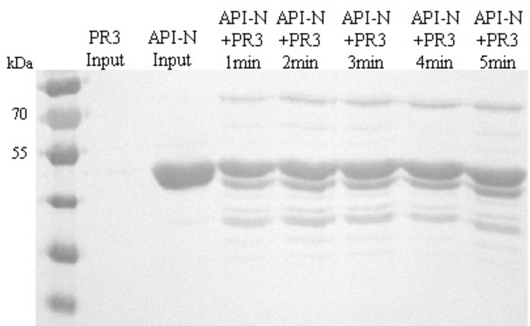
kDa
70
55
PR3 Input
API-N Input
API-N +PR3 1min
API-N +PR3 2min
API-N +PR3 3min
API-N +PR3 4min
API-N +PR3 5min

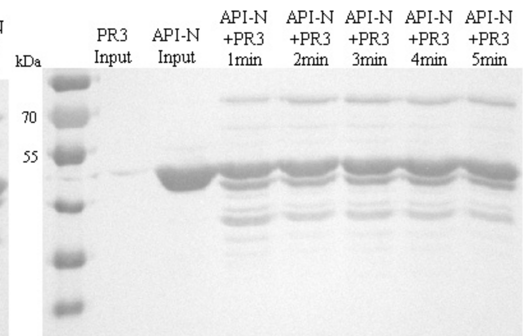
kDa
70
55
PR3 Input
API-N Input
API-N +PR3 1min
API-N +PR3 2min
API-N +PR3 3min
API-N +PR3 4min
API-N +PR3 5min

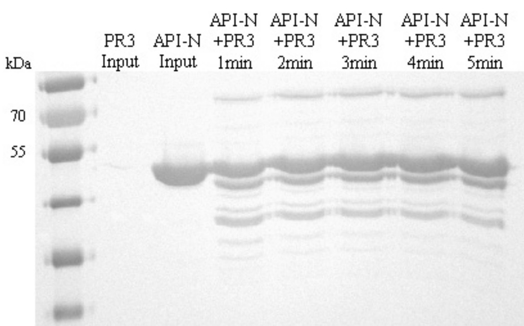
kDa
70
55
PR3 Input
API-N Input
API-N +PR3 1min
API-N +PR3 2min
API-N +PR3 3min
API-N +PR3 4min
API-N +PR3 5min

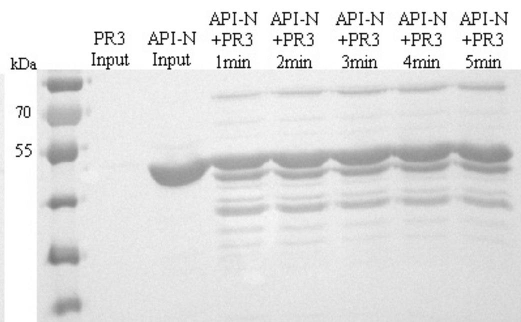
kDa
70
55
PR3 Input
API-N Input
API-N +PR3 1min
API-N +PR3 2min
API-N +PR3 3min
API-N +PR3 4min
API-N +PR3 5min

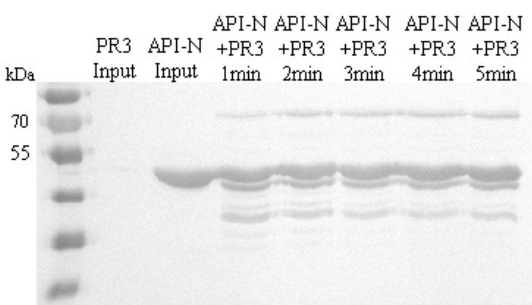
kDa
70
55
PR3 Input
API-N Input
API-N +PR3 1min
API-N +PR3 2min
API-N +PR3 3min
API-N +PR3 4min
API-N +PR3 5min

Figure 23: API-N+PR3 Kinetic Analysis Plots.

Gel-based kinetic analysis of API-N and PR3 binding showing the progression of the complex formation between the two proteins over 5 minutes (trials 1-5). These graphs correspond to the immunoblots shown in Figure 20.

API-N+PR3 Trial 1

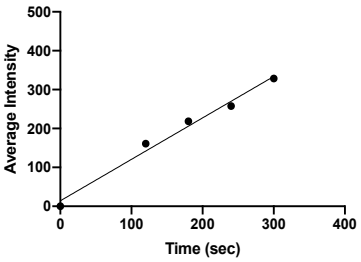

Y = 1.066*X + 14.06

R^2 = 0.9853

API-N+PR3 Trial 2

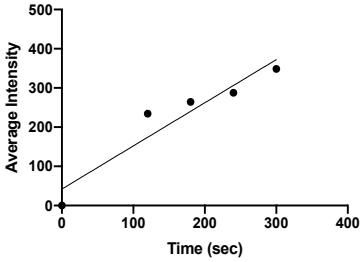

Y = 1.101*X + 42.09

R^2 = 0.9037

API-N+PR3 Trial 3

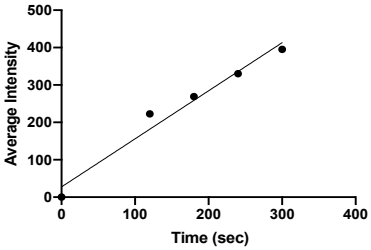

Y = 1.285*X + 27.44

R^2 = 0.9683

API-N+PR3 Trial 4

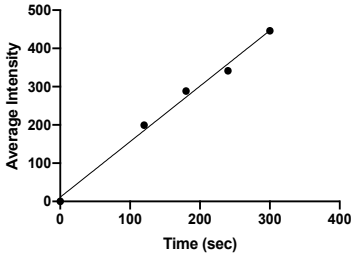

Y = 1.452*X + 11.13

R^2 = 0.9920

API-N+PR3 Trial 5

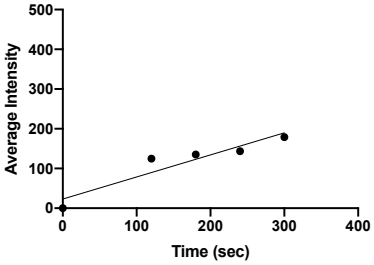

Y = 0.5553*X + 23.17

R^2 = 0.8828

Table 8: k_2^* Values for API-WT and API-N.

API-N yielded a second order rate constant that was not significantly different than API-WT, with a p-value of 0.8244 (unpaired t-test).

Protein Variant	k_2^*(10^5 arbitrary intensity units^{-1}s^{-1})	Significant Difference from API-WT
API-WT	1.16 ±0.53	
API-N	1.10 ±0.34	Not Significant; p=0.8244

5.10 API-N-PR3 k_2 Calibration Using Known Concentrations of API-N

The calculated k_2^*, which was based on arbitrary band intensity units, needed to be calibrated with known concentrations of API to obtain the true k_2 value. However, this was only done for the k_2 of the API-N-PR3 interaction and not API-WT-PR3, due to COVID-19 closures. Figure 24 shows the API-N calibration immunoblot with decreasing concentrations of API-N from 2μM to 0.0625μM. Unlike prior immunoblots, the bands in this calibration test were quantified by measuring the bands' volume, rather than their mid-line intensities. The API-N-PR3 complexing trials (Figure 22) were also re-quantified using the volume method, to ensure consistency within the calibration. A standard curve was made from the calibration plot (Figure 25), which was then used to determine the concentrations of the API-N-PR3 complex bands.

To calculate the k_2 value, a previously described method[60] was utilized. Per this method, a $\ln(P_0/P_t)$ versus time curve was generated where P_0 is the starting concentration of PR3 in the assay (1μM) and P_t is the remaining unreacted PR3 (Figure 26). The slope of the curve was then divided by the concentration of API (10μM) to calculate the k_2 value for each trial. All those values were then averaged to produce a mean k_2 of 0.68×10^3 M^{-1} s^{-1} $\pm$ 0.34×10^3 (±50%).

Figure 24: API-N Calibration Immunoblot.

Purified recombinant API-N was loaded at decreasing concentrations starting with 2μM.

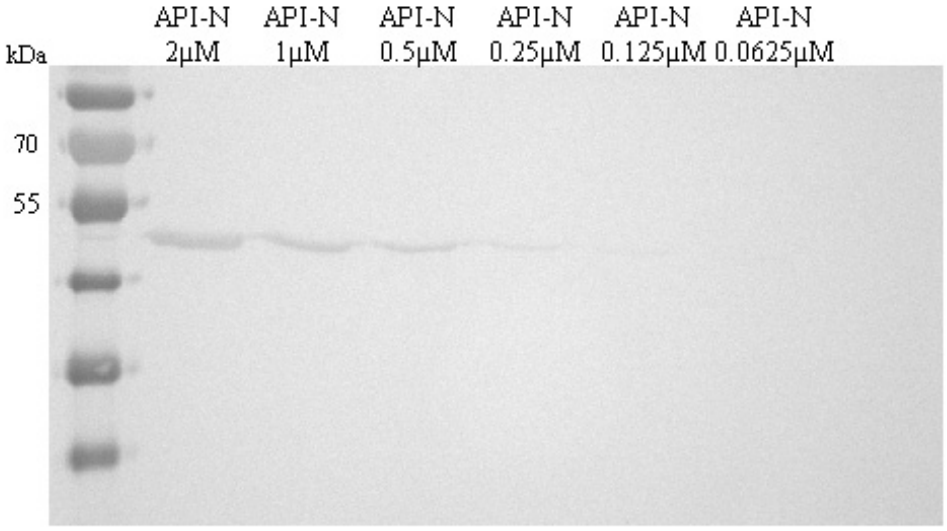
API-N 2μM
API-N 1μM
API-N 0.5μM
API-N 0.25μM
API-N 0.125μM
API-N 0.0625μM
kDa
70
55

Figure 25: API-N Standard Curve of Densitometric Band Volume versus Concentration (μM).

This standard curve was used to calibrate the gel-based kinetic analysis of the API-N+PR3 reactions.

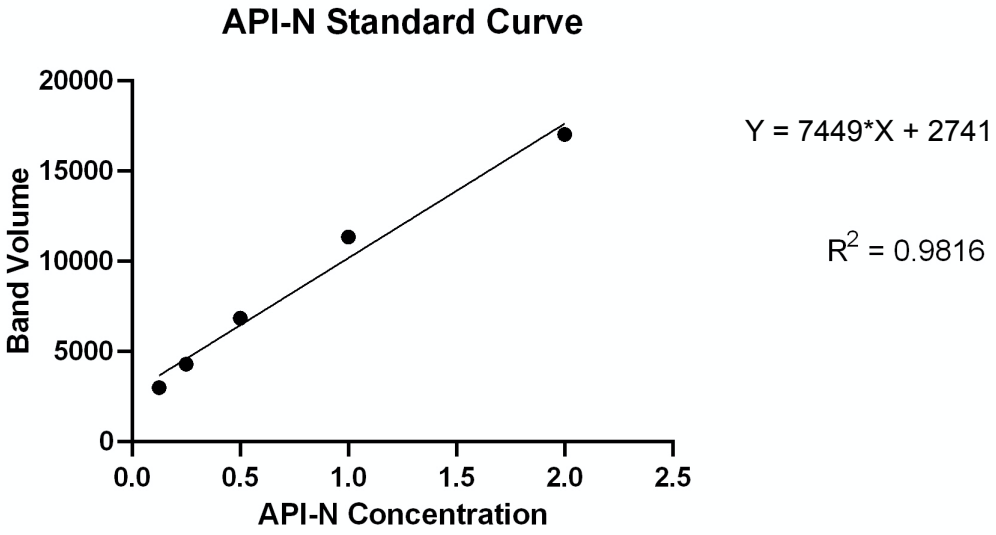
API-N Standard Curve
Band Volume
20000
15000
10000
5000
0
0.0
0.5
1.0
1.5
2.0
2.5
API-N Concentration
Y = 7449*X + 2741
R2 = 0.9816

Figure 26: Example of Calibrated API-N+PR3 Gel-Based Kinetic Curve.

This was the curve for the first trial, where P_0 is the starting concentration of PR3 in the assay (1μM) and P_t is the remaining unreacted PR3. Other trials are not shown in this thesis.

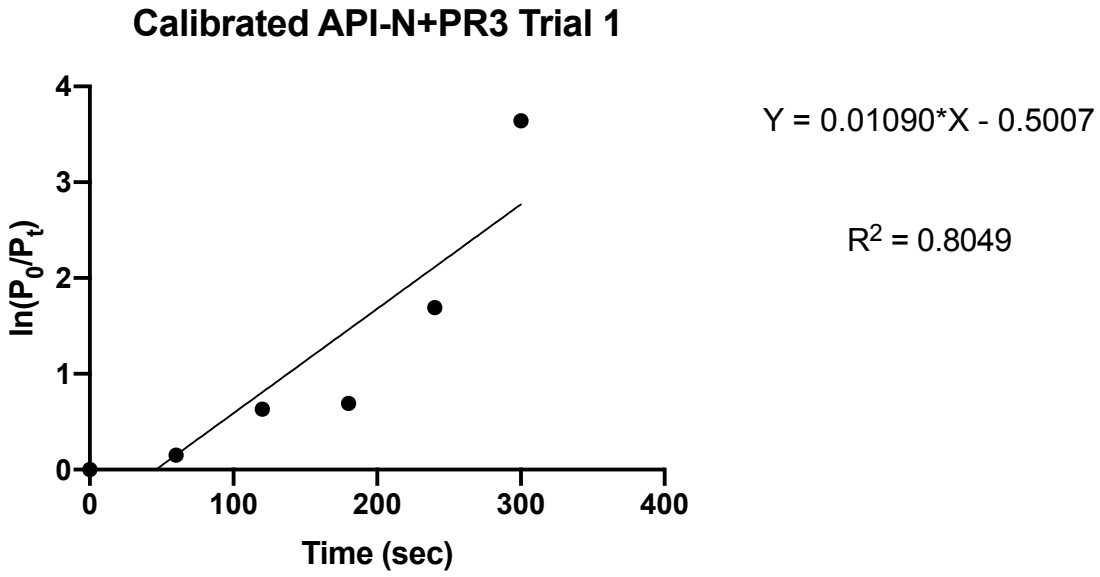
Calibrated API-N+PR3 Trial 1
ln(P0/Pt)
Time (sec)
0
1
2
3
4
0
100
200
300
400
Y = 0.01090*X - 0.5007
R2 = 0.8049

6 Discussion

The overall aim of this project was to explore a possible novel therapeutic approach for GPA, an autoimmune vasculitis whose pathology involves unregulated PR3. To do so, we chose to manipulate the endogenous PR3 inhibitor API, a member of the serpin superfamily. However, API is a better inhibitor of HNE than PR3 with k_2 values of $6.5x10^7$ and $4.5x10^5$ $M^{-1}s^{-1}$ respectively.[50,51] Thus, we endeavored to engineer a novel API variant that was more specific and reactive with PR3, thus shifting API's specificity away from HNE. To achieve this goal, we manipulated the RCL of API. This is the active site of the protein that contains the scissile bond P1-P1', which is cleaved by target proteinases, triggering a massive conformational change leading to their inhibition. This approach was chosen based on the precedent set by the Pittsburgh mutation, in which the methionine at position 358 of the RCL was substituted with an arginine resulting in API-R.[45] This variant had a shift in target proteinase specificity from HNE to thrombin and fXIa resulting in a bleeding disorder in the child that first acquired this mutation.[45] This case provided insight into the possibility of engineering other serpins to target specific proteinases. Our lab has had some previous success in this area, in studies in which a P7-P3 hypervariable API M358R library was inserted into a phage display system, and screened to yield two novel mutants with 2-fold increases in k_2 values for thrombin.[60]

6.1 Results and Limitations of Phage Display

This project utilized the same phage display approach, however, we randomized the P4-P1' positions within the RCL of API, and used PR3 to screen or biopan this API-P4P1' phage library. As mentioned earlier, these 5 positions were chosen to be

randomized as they were previously shown to produce variants of SERPINB1 with improved specificities to PR3 over HNE.[54] However, there was another consideration that also limited the number of codons in the RCL that could be randomized. This important factor was called the multiplicity, which was the number of times a different serpin possibility at the amino acid level was expressed in the biopanned phage.[59] There were 64 possibilities per codon that were generated by only 21 amino acids or stop outcomes, giving an average of ~3.05/64 possibilities. The biopanning protocol employed 10^9 amplified phage. Therefore, randomizing five codons will give the following maximum theoretical multiplicity:

$$10^9/(\frac{3.05}{64})^5 \approx 245$$

Since the phage library used for biopanning had already been biologically amplified by infection of *E. coli*, each original packaged library member would have 100 copies minimum, based on the manufacturer's guidelines.[59] This reduced the maximum multiplicity to ~2.45. The T7Select manufacturers recommended a multiplicity of 100 to ensure that rare variants were not missed in biopanning. However, our lab has shown that API libraries hypervariable from P7-P3 (five codons), P13-P8 (six codons, with P12 fixed as alanine), and P2-P3' (five codons, with P1 fixed as arginine) resulted in decreased diversity and the identification of variants inhibiting the proteinase of interest being present in the Round 4 or 5 populations, despite the sub-optimal multiplicity. [59,60] Based on the evidence in the literature, and limitations to multiplicity, a maximum of 5 residues (P4-P1') were randomized. The phage libraries were then biopanned a total of 5 consecutive rounds, with each resulting library serving as the starting material for the next

round. The choice to perform 5 rounds of biopanning was made based on data from our group and others that showed this number was sufficient in producing a phage library with desirable properties and selective pressure.[52,60]

Another important aspect of phage library screening that researchers must consider is the depth of their library. That is to say, "is the library being screened representative of the total number of variants that could possibly exist within it?" Within this project, it became evident to us that our API-P4P1' phage library screens did not probe all the possible variants that could be produced from randomizing 5 residues in the RCL. Theoretically, by randomizing 5 positions that could produce 21 amino acids in each of them, 4,084,101 API variants should be generated. However, when the plasmid library was inserted into the phage, tittered and deep-sequenced, only 7,495 (~0.002% of all possible variants) unique nucleic acid variants were expressed. This reduction in library depth could be a result of two limitations: the transformation efficiency of the competent *E. coli* cells initially used in the mass plasmid propagation of the library; and the deep-sequencing parameters that we employed. We used chemically competent *E. coli* DH5α cells. A more appropriate choice would have been to use electrocompetent strains that were better suited for large library transformations. Such cells have a high transformation efficiency of $>1x10^{10}$ colony forming units (cfu)/µg compared to chemically competent cells that have a medium transformation efficiency of $1x10^{8}$ (cfu)/µg. Furthermore, when NGS was employed, we analyzed our samples on the same plate in parallel with samples from other labs, to minimize cost. The resulting number of

sequences reported comprised 1% of the total possible sequences on the plate, which also reduced the number of unique variants we ultimately considered.

Even though these limitations were present, we found compelling data that made us proceed to kinetically characterize the enriched API variants. After 5 rounds of biopanning, the API-P4P1' phage library resulted in the enrichment of API-DA (API P357D/M358A), as seen in Figure 5. Moreover, this variant was the most abundant in the Round 5 screen of the API-P2P1 library, a previously made less hypervariable library that was used as a preliminary test for this project. API variants expressed on the surface of phage, exist in a fusion form with phage coat protein 10B, rather than a soluble one.[59,60] These fusion proteins may not exist in the correct orientation or conformation to bind with the target proteinases. Thus, we used the API-P2P1 phage library to ensure that PR3 applied selective pressure to the phage, therefore allowing us to proceed to the larger library, API-P4P1'. The convergence of two independent screens towards API-DA, and its novelty within the literature, made it a protein of interest. Based on this data and time constraints, we chose to proceed with the expression, purification and characterization of the API-DA variant.

6.2 Combining Phage Display with Bacterial Lysate Screening

To eliminate bias resulting from only selecting API-DA for further analysis, we performed a mass lysate screen that was developed within our lab.[70] This screening technique was previously used to distinguish the thrombin-specific API-R from other non-inhibitory API variants in *E. coli* lysates containing soluble recombinant API. By using thrombin-coated microtiter wells, the investigators were able to detect the API-R

variant functionally, in a library that expressed API-R at a 1:99 ratio with non-inhibitory variants. This approach was then further employed to screen a library encoding hypervariable API with all possibilities at codons 352-358, which yielded novel thrombin-inhibitory variants. Another library expressing all possible codons at position 347 was also probed using this modality and yielded the wild-type, 6 different functional variants, one partially active variant, and two variants with no thrombin-inhibitory activity.

In this project, the 3rd round phage library lysates, comprising soluble forms of the variants selected within the phage-display screen, were expressed and screened against PR3. The Round 3 lysate was chosen over the Round 5 as the API-DA variant made up approximately 32% and 57% of each library, respectively. This choice allowed us to use a library of API variants that had been subjected to sufficient selective pressure, while reducing the possibility of saturating the mass lysate screen with API-DA. Furthermore, this approach allowed us to screen non-tethered API variants. As previously described, the employed phage expresses fusion forms of API, which may hinder the interaction of some variants with PR3. Although such variants were still selected through phage display, they may possess better binding qualities to PR3 in their soluble forms. Therefore, this assay provided us a phage display-independent approach to screen our library. This yielded another novel variant: API-N (API S359N), which was the second most enriched variant within the API-P4P1' phage-display screen. Its selection within this screen over API-DA could be due to its expression as a soluble rather than a fusion protein, as

mentioned earlier. Its selection within two different screening techniques also made it a variant of interest for further analysis.

6.3 What About Other Variants?

Although the variants AISSS, AISTS and AINTS were the 3rd, 4th and 5th most abundant variants in Round 5 of the phage display screen, their abundance levels were much lower than those of API-DA and API-N. Their enrichment levels over the 5 rounds were also not as consistent as API-DA and API-N, as their abundance began to decrease after Round 3 of screening (Figure 5 and Table 3). Finally, none of these variants were selected by the mass lysate screen. For these reasons, coupled with the contrasting abundance and consistency of selection of API-DA and API-N, the variants AISSS, AISTS and AINTS were not considered for further analysis.

6.4 Assessing the Rate of PR3 Inhibition by API

To assess the rate of PR3 inhibition by API, first we performed serpin-proteinase gel-based complexing assays. Due to the nature of the covalent linkage between serpins and their target proteinases, the serpin-proteinase complex could be visualized on an SDS-PAGE gel. Based on these preliminary qualitative experiments, we observed complex formation between PR3 and recombinant API-WT and API-N, but not API-DA (Figures 15-17). However, the lack of a visible complex on a gel did not definitively eliminate API-DA as a possible inhibitor. Thus, k_2 determination experiments were done. At first, we chose to adapt the protocol used by Korkmaz et al. and Sinden et al. to calculate the k_2 of API-PR3 binding.[66,67] Their approach employed PR3-specific FRET substrates, as Korkmaz et al. had shown that these substrates were more specific towards PR3 than

other commercial products (i.e. chromogenic substrates). However, this approach was not successful in producing linear plots to generate a second order rate constant. Even though we attempted to reproduce their design, not all reagents were the same. Both groups used PD-API-WT, which may have had higher activity than our recombinant API stock. Our FRET substrates also slightly differed, due to commercial availability. Sinden et al. used the FRET substrate Abz-Val-Ala-Asp-Nva-Ala-Asp-Arg-Gln-EDDnp, whereas we used Abz-Val-Ala-Asp-Nva-Arg-Asp-Arg-Gln-EDDnp.[67] Their substrate had an alanine after the norvaline at the cleavage site, while ours had an arginine residue. Steps were then taken to adjust the experiment. Several trials were done by changing the molar ratio of API:PR3, where API was used in 5:1, 10:1 and 20:1 ratios. Furthermore, the absolute concentrations of the proteins were also varied. Although these attempts were made to optimize this approach, none of the trials yielded a linear plot over time to calculate a k_2 value. As a result, we chose to move on to gel-based kinetic analysis instead.

With our new approach, we were able to produce immunoblots showing increasing complex formation over time. This observation allowed us to calculate k_2^* values for recombinant API-WT and API-N that were based on arbitrary band intensity units. We found that there was no significant difference between the k_2^* of API-WT and API-N. This finding was supported by the qualitative gel-based complexing assays, that showed no discernable differences between the complex formation of PR3 with API-WT and API-N. This k_2^* value was then calibrated for API-N with known concentrations of API-N. However, the calibrated second order rate constant was not determined for API-WT due to COVID-19 closures. Therefore, our observations were drawn from the k_2^*.

Moreover, even though both API-WT and API-N bound to PR3 at the same rate, API-N could still be a viable candidate for a protein therapeutic agent if its specificity for HNE was reduced. However, kinetic analysis between API and HNE was not completed due to COVID-19 restrictions (see Section 7.2).

6.5 Slower Rates of Inhibition by Recombinant His-Tagged API than Glycosylated Isoforms

When determining the k_2^* of API-WT, we compared it to the reported k_2 within the literature. Korkmaz et al. and Sindern et al. had reported k_2 values of $4.5x10^5$ and $9.2x10^5$ $M^{-1}s^{-1}$, respectively.[50,67] We found that API-WT had a k_2^* of $1.16x10^5$ arbitrary intensity $units^{-1}s^{-1}$. However, we realized that the apparent similarity in order of magnitude of k_2^* of API-N of $1.10x10^5$ arbitrary intensity $units^{-1}s^{-1}$, compared to the published values above, was merely coincidental, with the true k_2 being $0.68x10^3$ $M^{-1}s^{-1}$ after calibration. If a proportional decrease in the k_2^* of API-WT was to be assumed (based on the aforementioned API-PR3 gel-based complexing assays), that would make our k_2 value at least 2 orders of magnitude lower than the published data. This difference could be explained by the use of different assays between us and the other groups. Our approach of using gel-based analysis introduced more variability between trials than FRET-based analysis. This variability could have occurred during the transfer of gel-components to nitrocellulose membranes for immunoblotting. To ensure complete transfer, the SDS-PAGE gels were stained with Coomassie Brilliant Blue dye and destained to ensure the disappearance of all bands. Another source of variability was the development of the immunoblots. Although steps were taken to ensure consistency, such as limiting

development times to 5 minutes maximum, some gels developed at a faster pace than others. This variability could have skewed our k_2^* values.

Another major difference between our approach and that of the other two groups, was the use of recombinant protein expressed in an *E. coli* system. We used non-glycosylated hexahistidine-tagged API-WT protein (mass ~48 kDa), whereas the other groups used commercially procured PD-API-WT (mass ~52 kDa). Generally, glycans are important for protein folding, stability, flexibility and signaling. In API, it has been shown that glycosylated and non-glycosylated isoforms have different folding and refolding patterns in *in vitro* studies. Unfolding was slowed down by glycosylation without affecting the rate of refolding. Moreover, unglycosylated API was more prone to heat-induced deactivation compared to PD-API-WT.[71] This finding indicates the importance of glycosylation to the stability of API. In addition, these glycans play an important role in preventing API polymerization, where reduced glycosylation could lead to increased polymerization rendering the protein inactive.[72]

Finally, our recombinant API proteins had an N-terminal hexahistidine-tag for purification purposes. This tag was not cleaved post-purification. One study has found that histidine-tagged recombinant API variants had higher thermal stability than their non-tagged counterparts.[73] This tag was also inserted at the N-terminus of the protein, away from the RCL. It was therefore unlikely that the histidine-tag interfered with binding of recombinant API to PR3, although this possibility cannot be excluded without further experimentation.

6.6 Observed and Theoretical Properties of API-DA and API-N

Although k_2 determination for API-DA binding to PR3 was not done due to COVID-19 closures, there were some observed differences between it and API-N from other experiments. Serpin-proteinase gel-based complexing assays showed us that while API-N formed complex similarly to API-WT, API-DA had a higher tendency to act as a substrate than the other two variants, suggesting that it was not a good inhibitor of PR3. However, API-DA was still highly selected within both our API-P4P1' and API-P2P1 phage display libraries. This high selection could be in part due to the presence of an alanine at the P1 position. Fu et al. had demonstrated through phage display experiments that PR3 preferred sequences with alanine in the P1 position, whereas HNE preferred valine.[52] They also found that PR3 slightly favoured sequences with serine in the P1' position compared to HNE. Serine was the natural amino acid at the P1' position in API, which was present in our API-DA variant. As mentioned in Section 1.7, amino acids upstream or downstream of the P1-P1' cleavage site could also have effects on the specificities of PR3 and HNE. Since both API-N and API-DA had those residues conserved from API-WT, they would not provide an explanation to the differences between the two variants.

However, Korkmaz et al. showed that there were differences in the charge-surface potentials of PR3 and HNE active sites.[74] The S2 subsite in PR3 was positively charged due to the presence of a lysine residue, as opposed to a leucine residue within HNE. Thus, a negatively charged residue at the P2 position of the substrate was preferred by PR3, as seen in API-DA where in the P2 position was an aspartic acid residue. There are,

however, two caveats that need to be considered. First, this data was generated from short substrates of around 8-10 amino acids in length, whereas our experiments utilized full length API. Second, we made the assumption that the cleavage site (P1-P1') remained at the same position and was not shifted within our variants. This assumption was made as the RCL environment around the assumed cleavage site was largely unchanged from wild-type. This assumption may not have been valid, with reference to the work done by Fu et al., who reported that the introduction of an arginine-glycine-glycine motif upstream of the cleavage site for HNE, shifted the P1-P1' site by 5 positions. It should be noted however, we found a consensus motif of AP - - S where the P4, P3 and P1' positions were conserved to alanine, isoleucine and serine, respectively, in our selected API-P4P1' library. This finding suggests that API's specificity to PR3 could be driven by the P2 and P1 residues, which complements the aforementioned studies where the profile of the P2 residue must match that of the PR3 S2 subsite, and the profile of the P1 residue must also be conducive to scissile bond cleavage.

Although COVID-19 closures prevented further experimentation with API-DA, independent confirmation that it could bind PR3 was provided by preliminary experiments in the bacterial lysate assay (Figure 7), in which it was demonstrated that API-DA bound PR3 more avidly than API-R but not as avidly as API-WT. This observation suggests several possible interpretations as to why API-DA was so vigorously selected in the phage display system, while not demonstrating vigorous complex formation with PR3 in gel-based assays. Firstly, complex formation could have been favoured in the context of the coat protein-API fusion protein to a greater extent

than in soluble form. Secondly, the prolonged reaction times and high affinity, biotin-assisted capture in the phage system could have facilitated the formation of covalently linked PR3-API complexes, even if API-DA is more suited to act as a substrate than an inhibitor in the known branched reaction pathway. Finally, it is possible that API-DA acted as a canonical or traditional "lock and key", rather than serpin-type inhibitor, to a greater extent than other variants, and could have formed a high affinity non-covalent complex with PR3 without reactive centre cleavage, or prior to it, in a stabilized encounter complex.

API-N, on the other hand, was largely unchanged from API-WT, as only the P1' residue was changed from a serine to an asparagine. Both these amino acids have polar uncharged side chains. There is no data in the literature that suggests this single mutation could have an impact on the specificities of either PR3 or HNE. To answer this question definitively, additional kinetic characterization of the API-N-HNE reaction needs to be done. It was clearly apparent, however, from the data that was generated that API-N behaved much more like API-WT with respect to covalent complex formation with PR3 than did API-DA.

Based on the evidence in the literature, API-DA may be more specific to PR3 than HNE (although this cannot be confirmed without performing k_2 determinations for the reactions between HNE and our two variants), compared to API-N. This speculative possibility was supported by API-DA's higher enrichment within our phage display experiments. However, serpin-proteinase gel-based complexing data suggested that API-DA was not a good inhibitor of PR3, as it acted as a substrate to the proteinase.

7 Conclusions and Future Directions

7.1 Conclusions

Within this project, we were able to demonstrate that PR3 was a viable "bait" proteinase within our phage display system, which allowed us to screen two hypervariable libraries of API (API-P2P1 and API-P4P1'). The libraries' diversity decreased over the 5 rounds of biopanning, yielding two enriched variants: API-DA and API-N, with the latter being further selected within a bacterial mass lysate screen. We were able to express variants within an *E. coli* expression system and produce purified soluble forms of those proteins. Although our kinetic characterization experiments were cut short due to the COVID-19 pandemic, we were able to demonstrate some inhibitory activity for these variants. We found that API-N and not API-DA formed inhibitory complexes with PR3 on SDS-PAGE gels, and that API-N had a similar k_2 value to recombinant API-WT.

7.2 Experiments Cut Short by COVID-19

The following experiments were planned to complete this master's project; however, we were unable to perform them due to laboratory restrictions as a result of the COVID-19 pandemic. First, we planned to determine the second order rate constant value for the binding of PR3 with API-DA, and HNE with API-WT, API-DA and API-N. These experiments would have allowed us to more accurately conclude which of the two novel variants was a better inhibitor of PR3 compared to HNE. Second, the gel-based kinetic analysis experiments of API-WT and API-DA were also to be calibrated with known concentrations of API, as was done for API-N. Finally, the experiments done using

recombinant API-WT were going to be repeated using PD-API-WT. The goal of these experiments was to determine if the size and glycosylation profile of API-WT could have an effect on its binding to PR3. This could have provided an explanation to the differences between our k_2 values and those published within the literature for wild-type API-PR3 reactions.

7.3 Future Directions

Future experiments could be designed to engineer API to more specifically inhibit PR3 using different approaches. Some of the API peptide sequences that have been found to have a high specificity towards PR3 could be inserted into the RCL of API and then kinetically characterized, such as the sequences VLLVSEVL and GLLVSGL, in which the predicted the cleavage site would be between the valine and serine.[52] The aim of such a study would be to ensure that these sequences would be viable in the larger context of an entire RCL, as the upstream and downstream environment of cleavage sites play a part in the serpin's binding to its target. Another possible manipulation would be to insert only the cleavage sites of those peptides into API's RCL, while also introducing aromatic residues upstream of the scissile bond, as seen in WWVAVS (P5-P1') which was highly selected by PR3 in a phage display screen.[52]

The aforementioned approaches are phage display-independent, however, future experiments could also enhance the screens done within this project. This includes a negative screen of the API-P4P1' library using HNE. If a variant was highly selected within both this screen and that with PR3, then it would be eliminated as a viable inhibitor, thus, providing more insight into identifying novel inhibitors of PR3. This

approach could be done separately from a PR3 screen, or it could be combined, by using negative selection to deplete libraries of HNE-reactive API variants and positive selection to enrich for PR3-reactive candidates. However, this approach remains API-dependent. Other API-independent approaches to inhibiting PR3 could also be explored. For instance, a library of recombinant antibody single chain variable fragments (ScFv) against PR3 could be expressed in a phage display system and probed with the same proteinase. Enriched candidates could then be further characterized through flow cytometry and kinetic analyses.[75] Such fragments have been previously identified against PR3, but not in an inhibitory capacity.[76] Furthermore, using ScFv over full-length recombinant protein has a few advantages. These include a reduced immunogenicity, lower retention time in non-target tissue, and these small fragments could also be coupled with other drugs to improve administration and inhibition of targets.[77]

8 References

1. Lutalo PMK, D'Cruz DP. Diagnosis and classification of granulomatosis with polyangiitis (aka Wegener's granulomatosis). Journal of Autoimmunity. 2014 Feb 1;48–49:94–8.
2. Gibelin A, Maldini C, Mahr A. Epidemiology and etiology of wegener granulomatosis, microscopic polyangiitis, churg-strauss syndrome and goodpasture syndrome: vasculitides with frequent lung involvement. Semin Respir Crit Care Med. 2011 Jun;32(3):264–73.
3. Alba MA, Jennette JC, Falk RJ. Pathogenesis of ANCA-associated pulmonary vasculitis. Semin Respir Crit Care Med. 2018 Aug;39(4):413–24.
4. Hilhorst M, Paassen P van, Tervaert JWC. Proteinase 3-ANCA Vasculitis versus Myeloperoxidase-ANCA Vasculitis. JASN. 2015 Oct 1;26(10):2314–27.
5. Pendergraft WF, Preston GA, Shah RR, Tropsha A, Carter CW, Jennette JC, et al. Autoimmunity is triggered by cPR-3(105-201), a protein complementary to human autoantigen proteinase-3. Nat Med. 2004 Jan;10(1):72–9.
6. Lyons PA, Rayner TF, Trivedi S, Holle JU, Watts RA, Jayne DRW, et al. Genetically distinct subsets within ANCA-associated vasculitis. N Engl J Med. 2012 Jul 19;367(3):214–23.
7. Jennette JC, Falk RJ. Pathogenesis of antineutrophil cytoplasmic autoantibody-mediated disease. Nat Rev Rheumatol. 2014 Aug;10(8):463–73.
8. Halbwachs-Mecarelli L, Bessou G, Lesavre P, Lopez S, Witko-Sarsat V. Bimodal distribution of proteinase 3 (PR3) surface expression reflects a constitutive

heterogeneity in the polymorphonuclear neutrophil pool. FEBS Lett. 1995 Oct 23;374(1):29–33.

9. Schreiber A, Busjahn A, Luft FC, Kettritz R. Membrane expression of proteinase 3 is genetically determined. J Am Soc Nephrol. 2003 Jan;14(1):68–75.
10. Witko-Sarsat V, Lesavre P, Lopez S, Bessou G, Hieblot C, Prum B, et al. A large subset of neutrophils expressing membrane proteinase 3 is a risk factor for vasculitis and rheumatoid arthritis. J Am Soc Nephrol. 1999 Jun;10(6):1224–33.
11. Csernok E, Ernst M, Schmitt W, Bainton DF, Gross WL. Activated neutrophils express proteinase 3 on their plasma membrane in vitro and in vivo. Clin Exp Immunol. 1994 Feb;95(2):244–50.
12. Bauer S, Abdgawad M, Gunnarsson L, Segelmark M, Tapper H, Hellmark T. Proteinase 3 and CD177 are expressed on the plasma membrane of the same subset of neutrophils. J Leukoc Biol. 2007 Feb;81(2):458–64.
13. Xiao H, Schreiber A, Heeringa P, Falk RJ, Jennette JC. Alternative complement pathway in the pathogenesis of disease mediated by anti-neutrophil cytoplasmic autoantibodies. Am J Pathol. 2007 Jan;170(1):52–64.
14. Schreiber A, Luft FC, Kettritz R. Membrane proteinase 3 expression and ANCA-induced neutrophil activation. Kidney International. 2004 Jun 1;65(6):2172–83.
15. Porges AJ, Redecha PB, Kimberly WT, Csernok E, Gross WL, Kimberly RP. Anti-neutrophil cytoplasmic antibodies engage and activate human neutrophils via Fc gamma RIIa. J Immunol. 1994 Aug 1;153(3):1271–80.

16. Kettritz R, Jennette JC, Falk RJ. Crosslinking of ANCA-antigens stimulates superoxide release by human neutrophils. J Am Soc Nephrol. 1997 Mar;8(3):386–94.
17. Hao J, Meng L-Q, Xu P-C, Chen M, Zhao M-H. p38MAPK, ERK and PI3K signaling pathways are involved in c5a-primed neutrophils for anca-mediated activation. PLoS One. 2012 May 31;7(5).
18. Wrann CD, Tabriz NA, Barkhausen T, Klos A, van Griensven M, Pape HC, et al. The phosphatidylinositol 3-kinase signaling pathway exerts protective effects during sepsis by controlling C5a-mediated activation of innate immune functions. J Immunol. 2007 May 1;178(9):5940–8.
19. Savage CO, Gaskin G, Pusey CD, Pearson JD. Anti-neutrophil cytoplasm antibodies can recognize vascular endothelial cell-bound anti-neutrophil cytoplasm antibody-associated autoantigens. Exp Nephrol. 1993 Jun;1(3):190–5.
20. Yang JJ, Preston GA, Pendergraft WF, Segelmark M, Heeringa P, Hogan SL, et al. Internalization of proteinase 3 is concomitant with endothelial cell apoptosis and internalization of myeloperoxidase with generation of intracellular oxidants. Am J Pathol. 2001 Feb;158(2):581–92.
21. Geetha D, Kallenberg C, Stone JH, Salama AD, Appel GB, Duna G, et al. Current therapy of granulomatosis with polyangiitis and microscopic polyangiitis: the role of rituximab. J Nephrol. 2015;28:17–27.

22. Ahlmann M, Hempel G. The effect of cyclophosphamide on the immune system: implications for clinical cancer therapy. Cancer Chemother Pharmacol. 2016 Oct 1;78(4):661–71.
23. Wang JY, Prorok G, Vaughan WP. Cytotoxicity, DNA cross-linking, and DNA single-strand breaks induced by cyclophosphamide in a rat leukemia in vivo. Cancer Chemother Pharmacol. 1993;31(5):381–6.
24. Williams DM. Clinical pharmacology of corticosteroids. Respiratory Care. 2018 Jun 1;63(6):655–70.
25. Fauci AS, Haynes BF, Katz P, Wolff SM. Wegener's granulomatosis: prospective clinical and therapeutic experience with 85 patients for 21 years. Ann Intern Med. 1983 Jan;98(1):76–85.
26. de Groot K, Harper L, Jayne DRW, Flores Suarez LF, Gregorini G, Gross WL, et al. Pulse versus daily oral cyclophosphamide for induction of remission in antineutrophil cytoplasmic antibody-associated vasculitis: a randomized trial. Ann Intern Med. 2009 May 19;150(10):670–80.
27. Harper L, Morgan MD, Walsh M, Hoglund P, Westman K, Flossmann O, et al. Pulse versus daily oral cyclophosphamide for induction of remission in ANCA-associated vasculitis: long-term follow-up. Ann Rheum Dis. 2012 Jun;71(6):955–60.
28. Randall KL. Rituximab in autoimmune diseases. Aust Prescr. 2016 Aug;39(4):131–4.

29. Korkmaz B, Poutrain P, Hazouard E, de Monte M, Attucci S, Gauthier FL. Competition between elastase and related proteases from human neutrophil for binding to alpha1-protease inhibitor. Am J Respir Cell Mol Biol. 2005 Jun;32(6):553–9.
30. Law RHP, Zhang Q, McGowan S, Buckle AM, Silverman GA, Wong W, et al. An overview of the serpin superfamily. Genome Biol. 2006;7(5):216.
31. Kaiserman D, Whisstock JC, Bird PI. Mechanisms of serpin dysfunction in disease. Expert Rev Mol Med. 2006 Dec 11;8(31):1–19.
32. Schechter I, Berger A. On the size of the active site in proteases. I. Papain. Biochem Biophys Res Commun. 1967 Apr 20;27(2):157–62.
33. Dahlen JR, Foster DC, Kisiel W. The inhibitory specificity of human proteinase inhibitor 8 is expanded through the use of multiple reactive site residues. Biochem Biophys Res Commun. 1998 Mar 6;244(1):172–7.
34. Gettins PGW, Olson ST. Inhibitory serpins. New insights into their folding, polymerization, regulation and clearance. Biochem J. 2016 01;473(15):2273–93.
35. Lawrence DA, Ginsburg D, Day DE, Berkenpas MB, Verhamme IM, Kvassman JO, et al. Serpin-protease complexes are trapped as stable acyl-enzyme intermediates. J Biol Chem. 1995 Oct 27;270(43):25309–12.
36. Huntington JA, Read RJ, Carrell RW. Structure of a serpin-protease complex shows inhibition by deformation. Nature. 2000 Oct 19;407(6806):923–6.

37. Tew DJ, Bottomley SP. Intrinsic fluorescence changes and rapid kinetics of proteinase deformation during serpin inhibition. FEBS Letters. 2001 Apr 6;494(1):30–3.

38. Lawrence DA, Olson ST, Palaniappan S, Ginsburg D. Engineering plasminogen activator inhibitor 1 mutants with increased functional stability. Biochemistry. 1994 Mar 29;33(12):3643–8.

39. Zhou A, Carrell RW, Huntington JA. The serpin inhibitory mechanism is critically dependent on the length of the reactive center loop. J Biol Chem. 2001 Jul 20;276(29):27541–7.

40. Hood DB, Huntington JA, Gettins PG. Alpha 1-proteinase inhibitor variant T345R. Influence of P14 residue on substrate and inhibitory pathways. Biochemistry. 1994 Jul 19;33(28):8538–47.

41. Yamasaki M, Arii Y, Mikami B, Hirose M. Loop-inserted and thermostabilized structure of P1-P1' cleaved ovalbumin mutant R339T. J Mol Biol. 2002 Jan 11;315(2):113–20.

42. Sim RB, Arlaud GJ, Colomb MG. Kinetics of reaction of human C1-inhibitor with the human complement system proteases C1r and C1s. Biochim Biophys Acta. 1980 Apr 11;612(2):433–49.

43. Kolarich D, Weber A, Turecek PL, Schwarz H-P, Altmann F. Comprehensive glyco-proteomic analysis of human alpha1-antitrypsin and its charge isoforms. Proteomics. 2006 Jun;6(11):3369–80.

44. Long GL, Chandra T, Woo SL, Davie EW, Kurachi K. Complete sequence of the cDNA for human alpha 1-antitrypsin and the gene for the S variant. Biochemistry. 1984 Oct 9;23(21):4828–37.
45. Owen MC, Brennan SO, Lewis JH, Carrell RW. Mutation of antitrypsin to antithrombin. alpha 1-antitrypsin Pittsburgh (358 Met leads to Arg), a fatal bleeding disorder. N Engl J Med. 1983 Sep 22;309(12):694–8.
46. Filion ML, Bhakta V, Nguyen LH, Liaw PS, Sheffield WP. Full or partial substitution of the reactive center loop of α-1-proteinase inhibitor by that of heparin cofactor II: p1 Arg is required for maximal thrombin inhibition. Biochemistry. 2004 Nov 1;43(46):14864–72.
47. Carrell RW. alpha 1-Antitrypsin: molecular pathology, leukocytes, and tissue damage. J Clin Invest. 1986 Dec;78(6):1427–31.
48. Crisford H, Sapey E, Stockley RA. Proteinase 3; a potential target in chronic obstructive pulmonary disease and other chronic inflammatory diseases. Respiratory Research. 2018 Sep 20;19(1):180.
49. Fujinaga M, Chernaia MM, Halenbeck R, Koths K, James MNG. The crystal structure of PR3, a neutrophil serine proteinase antigen of Wegener's granulomatosis antibodies. Journal of Molecular Biology. 1996 Aug 16;261(2):267–78.
50. Korkmaz B, Lesner A, Guarino C, Wysocka M, Kellenberger C, Watier H, et al. Inhibitors and antibody fragments as potential anti-inflammatory therapeutics

targeting neutrophil proteinase 3 in human disease. Pharmacol Rev. 2016;68(3):603–30.

51. Beatty K, Bieth J, Travis J. Kinetics of association of serine proteinases with native and oxidized alpha-1-proteinase inhibitor and alpha-1-antichymotrypsin. J Biol Chem. 1980 May 10;255(9):3931–4.
52. Fu Z, Thorpe M, Akula S, Chahal G, Hellman LT. Extended cleavage specificity of human neutrophil elastase, human proteinase 3, and their distant ortholog clawed frog PR3—Three elastases with similar primary but different extended specificities and stability. Front Immunol. 2018 Oct 16;9.
53. Groutas WC, Ruan S, Kuang R, Hook JB, Sands H. Inhibition of human leukocyte proteinase 3 by a novel recombinant serine proteinase inhibitor (LEX032). Biochem Biophys Res Commun. 1997 Apr 28;233(3):697–9.
54. Jégot G, Derache C, Castella S, Lahouassa H, Pitois E, Jourdan ML, et al. A substrate-based approach to convert SerpinB1 into a specific inhibitor of proteinase 3, the Wegener's granulomatosis autoantigen. FASEB J. 2011 Sep;25(9):3019–31.
55. Zani M-L, Baranger K, Guyot N, Dallet-Choisy S, Moreau T. Protease inhibitors derived from elafin and SLPI and engineered to have enhanced specificity towards neutrophil serine proteases. Protein Sci. 2009 Mar;18(3):579–94.
56. Liu T, Fu G, Luo X, Liu Y, Wang Y, Wang RE, et al. Rational design of antibody protease inhibitors. J Am Chem Soc. 2015 Apr 1;137(12):4042–5.

57. Guarino C, Gruba N, Grzywa R, Dyguda-Kazimierowicz E, Hamon Y, Łęgowska M, et al. Exploiting the S4-S5 specificity of human neutrophil proteinase 3 to improve the potency of peptidyl di(chlorophenyl)-phosphonate ester inhibitors: A kinetic and molecular modeling analysis. J Med Chem. 2018 Mar 8;61(5):1858–70.
58. Bratkovič T. Progress in phage display: evolution of the technique and its applications. Cell Mol Life Sci. 2010 Mar 1;67(5):749–67.
59. de Souza LR, Scott BM, Bhakta V, Donkor DA, Perruzza DL, Sheffield WP. Serpin phage display: the use of a T7 system to probe reactive center loop libraries with different serine proteinases. Methods Mol Biol. 2018;1826:41–64.
60. Scott BM, Matochko WL, Gierczak RF, Bhakta V, Derda R, Sheffield WP. Phage display of the serpin alpha-1 proteinase inhibitor randomized at consecutive residues in the reactive centre loop and biopanned with or without thrombin. PLOS ONE. 2014 Jan 10;9(1):e84491.
61. Pannekoek H, van Meijer M, Schleef RR, Loskutoff DJ, Barbas CF. Functional display of human plasminogen-activator inhibitor 1 (PAI-1) on phages: novel perspectives for structure-function analysis by error-prone DNA synthesis. Gene. 1993 Jun 15;128(1):135–40.
62. Fukunaga K, Taki M. Practical tips for construction of custom Peptide libraries and affinity selection by using commercially available phage display cloning systems. J Nucleic Acids. 2012;2012:295719.

63. Berkenpas MB, Lawrence DA, Ginsburg D. Molecular evolution of plasminogen activator inhibitor-1 functional stability. EMBO J. 1995 Jul 3;14(13):2969–77.

64. T7Select®10-3 Cloning Kit | 70550 [Internet]. [cited 2019 Jan 30]. Available from: http://www.emdmillipore.com/CA/en/product/T7Select10-3-Cloning-Kit,EMD_BIO-70550#anchor_USP

65. Merril CR. Gel-staining techniques. Meth Enzymol. 1990;182:477–88.

66. Korkmaz B, Attucci S, Juliano MA, Kalupov T, Jourdan M-L, Juliano L, et al. Measuring elastase, proteinase 3 and cathepsin G activities at the surface of human neutrophils with fluorescence resonance energy transfer substrates. Nature Protocols. 2008 Jun;3(6):991–1000.

67. Sinden NJ, Baker MJ, Smith DJ, Kreft J-U, Dafforn TR, Stockley RA. α-1-antitrypsin variants and the proteinase/antiproteinase imbalance in chronic obstructive pulmonary disease. Am J Physiol Lung Cell Mol Physiol. 2015 Jan 15;308(2):L179-190.

68. Sutherland JS, Bhakta V, Sheffield WP. The appended tail region of heparin cofactor II and additional reactive centre loop mutations combine to increase the reactivity and specificity of alpha1-proteinase inhibitor M358R for thrombin. Thromb Haemost. 2007 Nov;98(5):1014–23.

69. Sutherland JS, Bhakta V, Filion ML, Sheffield WP. The transferable tail: fusion of the N-terminal acidic extension of heparin cofactor II to alpha1-proteinase inhibitor M358R specifically increases the rate of thrombin inhibition. Biochemistry. 2006 Sep 26;45(38):11444–52.

70. Bhakta V, Gierczak RF, Sheffield WP. Expression screening of bacterial libraries of recombinant alpha-1 proteinase inhibitor variants for candidates with thrombin inhibitory capacity. Journal of Biotechnology. 2013 Dec 1;168(4):373–81.
71. Kwon KS, Yu MH. Effect of glycosylation on the stability of alpha1-antitrypsin toward urea denaturation and thermal deactivation. Biochim Biophys Acta. 1997 Jun 6;1335(3):265–72.
72. McCarthy C, Saldova R, Wormald MR, Rudd PM, McElvaney NG, Reeves EP. The role and importance of glycosylation of acute phase proteins with focus on alpha-1 antitrypsin in acute and chronic inflammatory conditions. J Proteome Res. 2014 Jul 3;13(7):3131–43.
73. Parfrey H, Mahadeva R, Ravenhill NA, Zhou A, Dafforn TR, Foreman RC, et al. Targeting a surface cavity of α1-antitrypsin to prevent conformational disease. J Biol Chem. 2003 Aug 29;278(35):33060–6.
74. Korkmaz B, Hajjar E, Kalupov T, Reuter N, Brillard-Bourdet M, Moreau T, et al. Influence of charge distribution at the active site surface on the substrate specificity of human neutrophil protease 3 and elastase. a kinetic and molecular modeling analysis. J Biol Chem. 2007 Jan 19;282(3):1989–97.
75. Zhang J, Valianou M, Simmons H, Robinson MK, Lee H-O, Mullins SR, et al. Identification of inhibitory scFv antibodies targeting fibroblast activation protein utilizing phage display functional screens. FASEB J. 2013 Feb;27(2):581–9.

76. Finnern R, Pedrollo E, Fisch I, Wieslander J, Marks JD, Lockwood CM, et al. Human autoimmune anti-proteinase 3 scFv from a phage display library. Clin Exp Immunol. 1997 Feb;107(2):269–81.

77. Ahmad ZA, Yeap SK, Ali AM, Ho WY, Alitheen NBM, Hamid M. ScFv antibody: principles and clinical application. Clin Dev Immunol. 2012;2012:980250.